

ORIGINAL RESEARCH

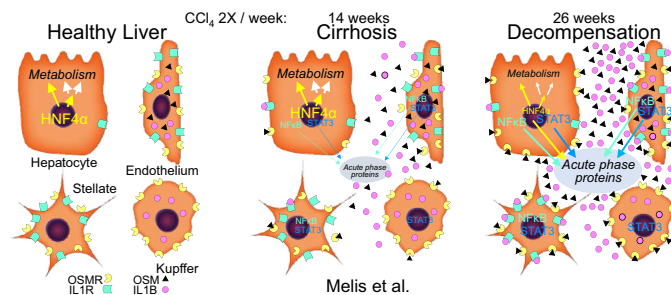
Mechanism and Effect of HNF4 α Decrease in a Rat Model of Cirrhosis and Liver Failure

Marta Melis,¹ Rebecca Marino,² Jianmin Tian,² Carla Johnson,² Rahil Sethi,³ Michael Oertel,^{2,4,5} Ira J. Fox,^{1,4,5} and Joseph Locker^{2,5}

¹Department of Surgery, University of Pittsburgh, Pittsburgh, Pennsylvania; ²Department of Pathology, University of Pittsburgh, Pittsburgh, Pennsylvania; ³Department of Biomedical Informatics, University of Pittsburgh, Pittsburgh, Pennsylvania; ⁴Pittsburgh Liver Research Center, University of Pittsburgh, Pittsburgh, Pennsylvania; and ⁵The McGowan Institute for Regenerative Medicine, University of Pittsburgh, Pittsburgh, Pennsylvania

Mechanism and effect of HNF4 α decrease in a rat model of cirrhosis and liver failure

Reduced HNF4 α characterized end-stage livers. The reduction was caused by a multicellular response to inflammatory cytokines that affected HNF4 α and numerous other hepatocyte transcription factors. The reduced HNF4 α still provided extensive phenotypic regulation and stimulated expression of acute phase proteins.



cmgh CELLULAR AND MOLECULAR GASTROENTEROLOGY AND HEPATOLOGY

SUMMARY

Reduced HNF4 α characterized end-stage livers. The reduction was caused by a multicellular response to inflammatory cytokines that affected HNF4 α and numerous other hepatocyte transcription factors. The reduced HNF4 α still provided extensive phenotypic regulation and stimulated expression of acute phase proteins.

BACKGROUND & AIMS: HNF4 α , a master regulator of liver development and the mature hepatocyte phenotype, is down-regulated in chronic and inflammatory liver disease. We used contemporary transcriptomics and epigenomics to study the cause and effects of this down-regulation and characterized a multicellular etiology.

METHODS: Progressive changes in the rat carbon tetrachloride model were studied by deep RNA sequencing and genome-wide chromatin immunoprecipitation sequencing analysis of transcription factor (TF) binding and chromatin modification. Studies compared decompensated cirrhosis with liver failure after 26 weeks of treatment with earlier compensated cirrhosis

and with additional rat models of chronic fibrosis. Finally, to resolve cell-specific responses and intercellular signaling, we compared transcriptomes of liver, nonparenchymal, and inflammatory cells.

RESULTS: HNF4 α was significantly lower in 26-week cirrhosis, part of a general reduction of TFs that regulate metabolism. Nevertheless, increased binding of HNF4 α contributed to strong activation of major phenotypic genes, whereas reduced binding to other genes had a moderate phenotypic effect. Decreased *Hnf4a* expression was the combined effect of STAT3 and nuclear factor kappa B (NF κ B) activation, which similarly reduced expression of other metabolic TFs. STAT/NF κ B also induced de novo expression of *Osmr* by hepatocytes to complement induced expression of *Osm* by nonparenchymal cells.

CONCLUSIONS: Liver decompensation by inflammatory STAT3 and NF κ B signaling was not a direct consequence of progressive cirrhosis. Despite significant reduction of *Hnf4a* expression, residual levels of this abundant TF still stimulated strong new gene expression. Reduction of HNF4 α was part of a broad hepatocyte transcriptional response to inflammation. (*Cell Mol Gastroenterol Hepatol* 2024;17:453–479; <https://doi.org/10.1016/j.jcmgh.2023.11.009>)

Keywords: STAT3; NF κ B; Oncostatin M Receptor (*Osmr*); Liver Epigenomics; *Hnf4a* Isoforms.

Cirrhosis is a chronic disease with multiple etiologies that include viral hepatitis, alcohol-related liver disease, and steatohepatitis. Complications or progression of cirrhosis to liver failure cause 1 million deaths per year worldwide.¹ Despite improved management² and extensive knowledge of cirrhosis pathways,^{3,4} the molecular networks that drive the late stages of cirrhosis and liver failure are unresolved. This lack of understanding is in part due to the high mortality in long-term animal experiments before they model the terminal stages of cirrhosis.

Observations suggest gradual progression until the liver becomes nonfunctional. Abundant fibrosis remodels the hepatic vasculature⁵; hepatocytes lose regenerative capacity and metabolic functions⁶; and there are persistent high levels of inflammation and oxidative stress.⁷ However, terminal processes frequently show an abrupt change in diseased but functional liver. Such acute-on-chronic failure is a sudden decompensation that often occurs in a context of multiorgan failure, with a high rate of short-term mortality.⁸ Viral hepatitis, alcoholic hepatitis, and acetaminophen intoxication are typical etiologies for acute-on-chronic failure.^{9–11} Nonalcoholic fatty liver disease has also become a prominent cause over the past decade.^{12–14}

Most acute-on-chronic cases present on a background of compensated cirrhosis that has been managed, even for decades, before liver failure occurs.² There are no clear markers that predict this lethal loss of liver function, although a recent analysis showed that inflammation, fibrosis, apoptosis, and senescence pathways characterized decompensation.¹⁵

Treatment of rodents with the hepatotoxin carbon tetrachloride (CCl₄) is a reliable model for mechanistic investigation of fibrosis and cirrhosis progression.¹⁶ Our group previously extended CCl₄ treatment of rats to 26 weeks with addition of phenobarbital to the drinking water to investigate progression to end-stage disease. After CCl₄ was terminated, the rats underwent terminal decompensation over the following 4–6 weeks that mirrored key molecular and pathophysiological features of human end-stage liver disease.^{17–19} These end-stage livers showed a decrease in HNF4 α , an abundant nuclear receptor transcription factor (TF) that acts as a master regulator of hepatocyte phenotype.²⁰ Decreased HNF4 α has also been observed in other rodent models without end-stage decompensation,^{21,22} as well as late-stage human cirrhosis and alcoholic hepatitis.^{23–25} Notably, the study of progression from early alcoholic steatohepatitis to alcoholic hepatitis with liver failure showed the strongest negative correlations between expression of *HNF4A* and inflammatory mediators *RELA*, *NFKB1*, and *STAT3*.²³ Normal HNF4 α expression is constitutive and does not undergo dynamic regulation, so decrease indicates a critical disruption of normal homeostasis.

In this study, we used long-term CCl₄ treatment of rats to investigate mechanism and regulatory effects of HNF4 α


depletion. The work is a direct extension of our previous articles,^{17–19} which provided detailed characterization of disease progression including histopathology. New RNA sequencing analysis confirmed the previous observations, demonstrating physiological levels of HNF4 α in compensated cirrhosis after 14 weeks but a 60% decrease in decompensated cirrhosis after 26 weeks of treatment. Analysis characterized differences between these disease stages and then compared 2 additional long-term models of rat liver fibrosis/cirrhosis, bile duct ligation (BDL) and thioacetamide (TAA) treatment. In parallel, chromatin immunoprecipitation sequencing analysis (chromatin immunoprecipitation sequencing) identified TF binding and chromatin modification. Because rat studies are limited, we used mouse databases to compile signaling pathways and cell-specific phenotypes. Although adaptive gene regulations may differ between species, the expression signatures derived from mouse provided important resources for characterizing rat disease progression. Together, these characterizations of the transcriptome and epigenome demonstrated cause and phenotypic impact of HNF4 α depletion. The deep molecular analyses also resolved specific contributions of hepatocytes, nonparenchymal cells (NPC), and inflammatory cells to pathogenesis.

Results

Hnf4a Transcription in Progressive Cirrhosis

Hnf4a regulation was compared in 3 experimental conditions, control and CCl₄ treatment for 14 or 26 weeks (CC14 and CC26, respectively). Whole livers were analyzed by RNA sequencing (RNA sequencing) and chromatin immunoprecipitation sequencing of TF and chromatin modifications²⁶ (Figure 1A and C, Supplementary Table 1). Nuclear receptor HNF4 α , the focus of this study, is among the most abundant hepatocyte TFs. Nuclear receptors typically bind to transcriptional enhancers that are distant from promoters and recruit p160 coactivators to activate chromatin surrounding the enhancer by acetylating histone H4 at lysine 5 (H4K5Ac). Analysis of H4K5Ac measured transcriptional activation and discriminated activating TF binding sites. Analysis of CEBP β , an abundant hepatocyte-enriched TF, discriminated enhancers at all distances from promoters. HNF4 α and CEBP β chromatin immunoprecipitation sequencing gave sharp non-overlapping peaks with

Abbreviations used in this paper: BDL, bile duct ligation; CCl₄, carbon tetrachloride; CC14, CC26, CCl₄-induced cirrhosis after 14 weeks or 26–28 weeks of treatment, respectively; ChIP-seq, chromatin immunoprecipitation sequencing; *Hnf4a-us*, the common promoter for lncRNA isoforms *Hnf4a-us1*, 2, and 3; IL, interleukin; NF κ B, nuclear factor kappa B; NPC, nonparenchymal liver cells; P1, the main *Hnf4a* promoter; P2, the minor *Hnf4a* promoter; RT-PCR, reverse transcriptase polymerase chain reaction; RNA-seq, RNA sequencing; TAA, thioacetamide; TF, transcription factor.

 Most current article

© 2023 The Authors. Published by Elsevier Inc. on behalf of the AGA Institute. This is an open access article under the CC BY-NC-ND license (<http://creativecommons.org/licenses/by-nc-nd/4.0/>).

2352-345X

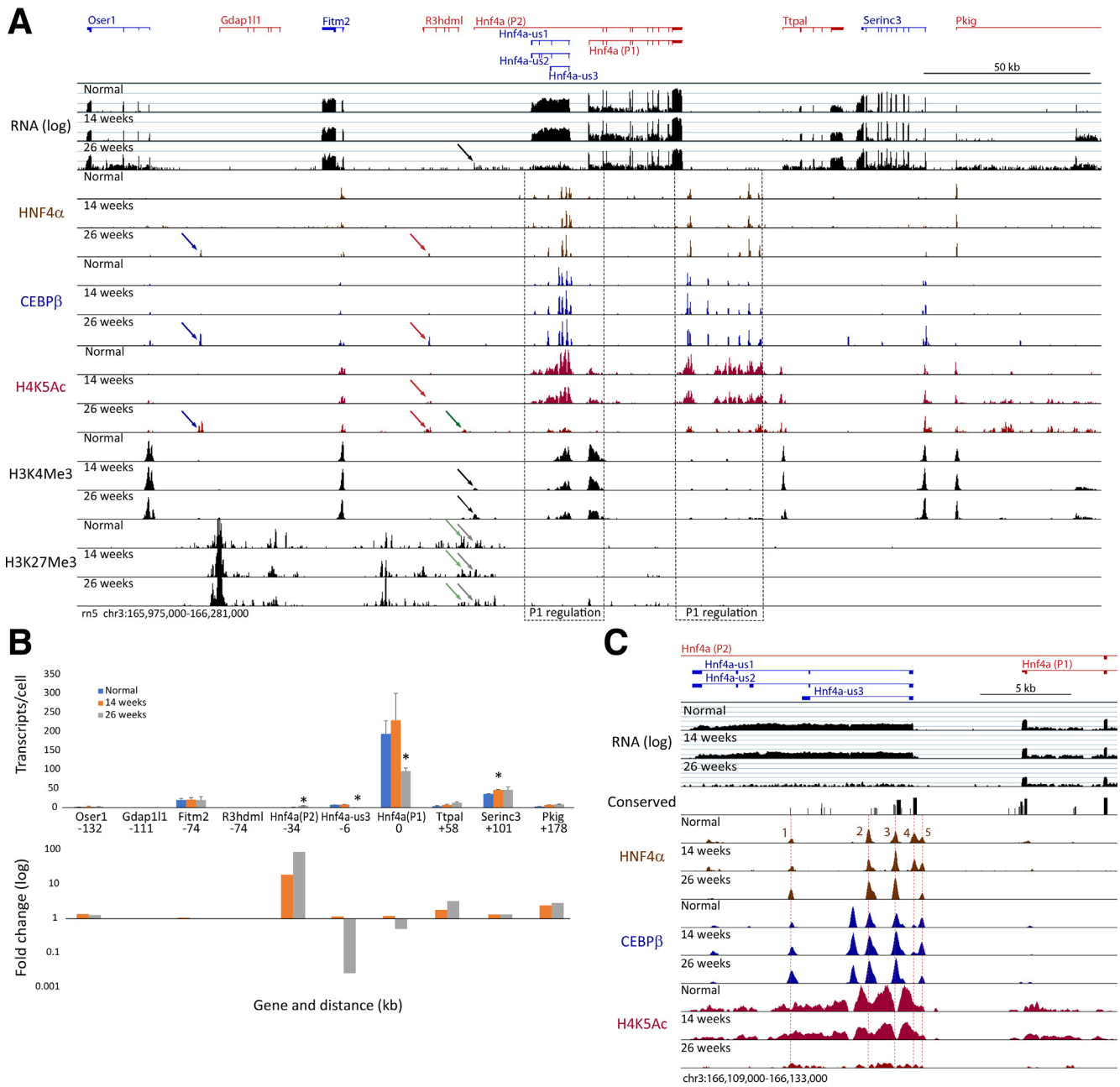
<https://doi.org/10.1016/j.jcmgh.2023.11.009>

~300 bp halfwidth, centered on their binding sites within enhancers. H4K5Ac was depleted over enhancers but surrounded them with broad ~800 bp peaks (Figure 1C). Two additional chromatin modifications were characterized. H3K4Me3 gave broad peaks downstream of active promoters, and repressing H3K27Me3 was scattered diffusely over inactive genes. In this study, HNF4 α and H4K5Ac peaks were tabulated and quantified. CEBP β , H3K4Me3, and H3K27Me3 provided additional qualitative information.

Analysis demonstrated 3 *Hnf4a*-related promoters. Abundant transcripts from the strong main *Hnf4a* promoter (P1) encode the main HNF4 α isoforms. A second strong promoter lies -6 kb upstream from P1 on the opposite DNA

strand. To define its transcripts, we cloned 3 spliced lncRNAs, collectively referred to as *Hnf4a-us*, that have a common first exon. Mouse and human genomes have similar upstream lncRNAs (*Hnf4aos* and *Hnf4-as1*, respectively) with the same promoter and first exon (Figure 2B), which splice to entirely different non-homologous exons in each species. Finally, transcripts from the weak minor *Hnf4a* promoter (P2) (-34 kb from P1) encode distinct *Hnf4a* isoforms first characterized in rat fetal liver²⁸ (Figure 2A).

Local enhancers comprised 2 clusters (super-enhancers), -5 to -13 kb upstream and +29 to +52 kb downstream from *Hnf4a*(P1) (Figure 1A and C). Many of these enhancers showed strong HNF4 α binding (Figure 1C), indicating



extensive transcriptional autoregulation. The target of these enhancer clusters is inferred by their proximity to *Hnf4a(P1)*, and both clusters showed H4K5Ac levels that changed in proportion to the level of transcription from this promoter. Despite changes in transcription and H4K5Ac, HNF4 α sites retained binding except Peak 4 (Figure 1C), which overlapped with the highly conserved *Hnf4a-us* promoter (Figure 2A).

Transcription in CC14 was essentially normal, but decompensated CC26 livers showed transcriptional changes at all 3 promoters (Figure 1A–C). Transcripts from the main P1 promoter were ~60% lower. *Hnf4a-us* transcripts, which normally extend through the upstream enhancer cluster, virtually disappeared. In contrast, transcripts from *Hnf4a(P2)* increased, a change that was accentuated in the plot of fold-change relative to normal. Consistent with this new expression, ChIPseq analysis suggested enhancer and promoter activation near P1 (arrows in Figure 1A). Because reciprocal expression of P1 and P2 transcripts was recently described in the decompensation of human alcoholic liver disease,²³ we quantified them using reverse transcriptase polymerase chain reaction (RT-PCR) and RNA-seq (Figure 2C–F). These analyses confirmed increased transcription from P2 but still much lower than P1 (~5 and ~100 transcripts/cell, respectively).

The levels of P2 transcripts and chromatin modification suggest a small liver cell population. Moreover, the isolation of the 2 isoform promoters from each other and their differential responses typically reflect function in the transcriptional environments of different cell types. Note that P2 shows repressive H3K27Me3 in all experimental conditions, suggesting repression in hepatocytes (Figure 1A). We therefore studied gene expression of NPC liver cells, which

were present at much lower levels than hepatocytes, and found clear expression of *Hnf4a* in RNA-seq data sets from mouse cholangiocytes,²⁹ which selectively expressed *Hnf4a(P2)* (Figure 2C and F). Thus, increased *Hnf4a(P2)* expression in CC26 likely reflected increased cholangiocytes, stimulation of expression in cholangiocytes, or a fraction of altered hepatocytes with partial transdifferentiation to cholangiocytes.^{30,31}

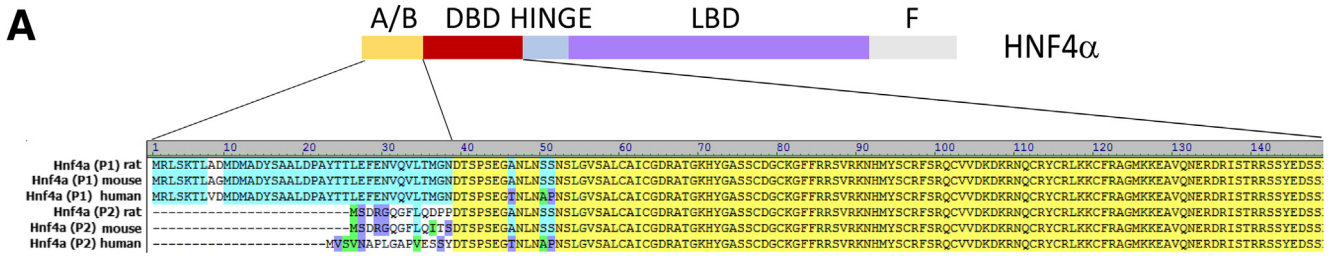
Binding of HNF4 α

For each experimental group, HNF4 α -binding peaks (Figure 3A, Supplementary Table 2) were scored for binding strength. Filtering out weak peaks and those without H4K5Ac binding left a set of ~20,000 active peaks. Plots comparing CC14 and CC26 with normal liver (Figure 3A) showed much greater change at 26 weeks, with increased or decreased HNF4 α binding at many sites. Subsequent analysis focused on peaks that showed the greatest changes at 26 weeks compared with normal.

Peak subsets with increased, decreased, or unchanged binding at 26 weeks were then analyzed with MEMEChip (Figure 3B), which compiled motifs related to the ideal DR1-binding site of HNF4 α (AGGTCAnAGGTCA) for all 3 groups. The high-significance motif signatures compiled for the unchanged- and decreased-binding subsets were identical, indicating the same average binding affinity in both sets. They closely matched prior global compilations of HNF4 α sites.^{20,34} Paradoxically, peaks with increased binding of HNF4 α yielded a shorter motif signature with much lower significance, indicating greater divergence and reduced binding affinity.

General scanning for binding HNF4 α binding motifs confirmed these observations, because less than half of the

Figure 1. (See previous page). ChIP-seq and RNA-seq analysis of progressive cirrhosis in the chromosome region around *Hnf4a*. (A) Survey of 306-kb region around *Hnf4a*. Main *Hnf4a* isoform transcript originated from promoter P1, antisense noncoding transcripts from promoter at -6 kb, and minor *Hnf4a* isoform transcripts from promoter P2 at -34 kb. In surrounding region, promoters of active genes (*Oser1*, *Fitm2*, *Hnf4a(P1)*, *Ttpal*, *Serinc3*, *Pkig*) show H3K4Me3 peaks, whereas 2 nonexpressed genes (*Gdap111*, *R3hdml*) are marked by repressing H3K27Me3. Note that major chromatin and transcript changes were selective for *Hnf4a(P1)* and did not affect the surrounding genes. *Hnf4a-us* transcripts include spliced lncRNAs and a high proportion of unspliced RNA (Figure 2D). RNA-seq is displayed on logarithmic scale to accommodate the wide range of transcript levels, which minimized the 60% drop in P1 transcripts. Presumptive regulatory regions for P1 (promoter elements, upstream and downstream enhancer clusters) are boxed. The 26-week tracks show reduced *Hnf4a(P1)* and nearly absent *Hnf4a-us* transcripts (spliced and unspliced). These changes coincided with marked reduction of H4K5Ac throughout both P1 regulatory regions. Note that H4K5Ac associated with other genes was maintained in all 3 experimental conditions; the retained acetylation just upstream of the *Ttpal* promoter marks the boundary of the *Hnf4a(P1)* regulatory region. Liver showed H3K27Me3, a chromatin marker of transcriptional repression, near the *Hnf4a(P2)* promoter (gray and gray-green arrows), which lacked expression, TF binding, and chromatin markers of activation in normal liver. As cirrhosis progressed, several changes coincided with activation of *Hnf4a(P2)*: The promoter showed exon 1 transcripts include new P2-exon 1 transcript and increased H3K4Me3 (black arrows). A region from -2.3 to 3.2 kb, where expression-related hypersensitive sites have been mapped,²⁷ showed new H4K5Ac (green arrow). Upstream regions near inactive *R3hdml* (red arrows) and *Gdap111* (blue arrows) showed new binding of HNF4 α , CEBP β , and H4K5Ac, suggesting enhancers that control expression from P2. (B) Gene expression. Quantifications are visualized as transcripts/cell (above) and fold-change relative to normal liver (below). Locations are relative to *Hnf4a(P1)* transcriptional start at 0 kb. There was little transcriptional change in this region, except for *Hnf4a(P1)*, *Hnf4a-us* (quantified from the common first exon of all spliced transcripts), and *Hnf4a(P2)*. The greatest transcriptional change was reduction of *Hnf4a(P1)* transcripts, although the ratios of change accentuated *Hnf4a-us* and *Hnf4a(P2)* transcripts. *t* tests, **P* vs normal liver, <.05. (C) Detail of proximal P1 regulatory region. HNF4 α -binding sites are numbered. Enhancers with TF binding sites appear as valleys between broad peaks of H4K5Ac-modified chromatin (red lines). HNF4 α -binding peaks 3 and 4 mark enhancers with high phylogenetic conservation, suggesting they are important controls of gene expression. Acetylation was greatly reduced in the 26-week livers, consistent with reduced transcription of *Hnf4a(P1)*, but binding of HNF4 α did not change except for peak 4. The Conserved track displays the phastCons13way compilation of vertebrates genomes. In parts A and C, ChIP-seq data are shown with a linear scale, and RNA-seq with a log₁₀ scale.



B

Peak 4 Vertebrate conserved block

Rat
Mouse
Human

```
TCTCCTCTTCTTCTCCCCACCTACCACCCAGGGTGCAGTGCAGGGGAAACCTGCACCTT
TCTCCTCTcCTTCTCCCCACCTACCACCCAGGGTGCAGTGCAGGGGAAACCTGCACCTT
TCTCCTaTcTtTCTCCCCACCTACCACctcGGGgAGGtGCAGaGaAAACtGgCAGCTT
```

LXR(3.0E-5)

```
ATCAAGACAAAGAACAAGTCTCGTGGGGCAAGGCAAGAGCCATGTCTACTTGGGG
ATCAAGACAAAGAACAAGTCTCGTGGGGCAAGAGCCAAAGtCATGTCTACTTGGGG
ATCAAGACAAAGAACAAGTCTCGTGGGgGaAAGaGCCAAAGCCATcTCTACTTGGGG
```

HNF4(3.0E-4) HNF4(1.7E-5)

```
TAGGGCC-TTCAGCTTCGCCCTTTGAATTTCAAATTTCCAATTTGGGACAAAGTCCTA
TAGGGCC-TTCAGtTCGCCCTTTGAaATTTCAAATTTCCAaTTTGGGACAAAGTCCTA
TAGGGCCcTTCAGtTtGCCCTTTGAaATTTCAAATTTCCAaTTTGGGACAAAGTCCTA
```

TATA INR (↑)

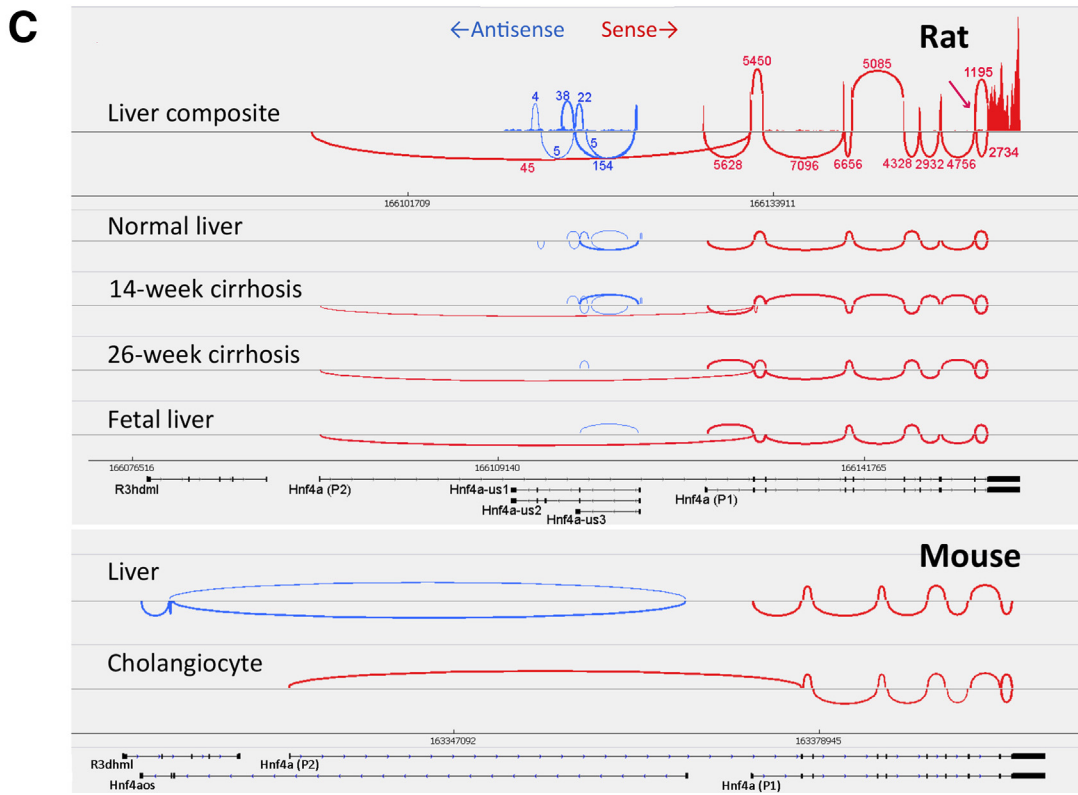
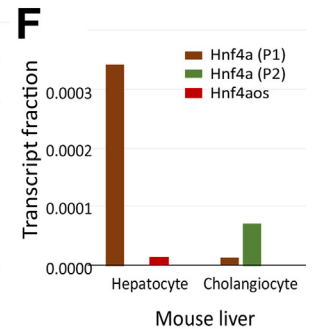
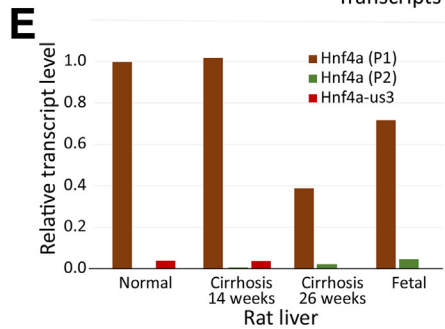
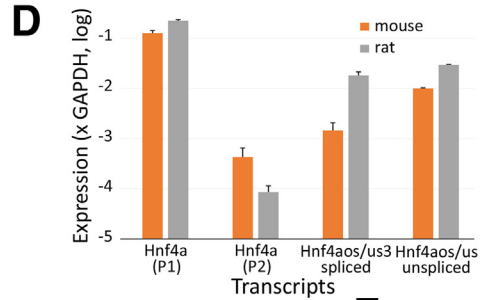
```
ACTATCTCACAATATAGGTCGCCCAACTGCTGACCAAACTCCAGTCCCAAGCAGCCACCTGG
ACTATCTCACAATATAGGTCGCCCAACTGCTGACCAAACTCCAGTCCCAAGCAGCCACCTGG
ACTATCTCACAATATAGGTCGCCCAACTGCTGACCAAACTCCAGTCCCAAGCAGCCACCaG-
```

CCTCAGACTAGCCTGGCTTTGCGCTTTCCTTTGGCAGCTCCCAAGCCGAGGGTAAAGAG
CCTYAGACTgSCCTGGCTTTGCGCTTTCCTTTGGCAGCTCCCAAGACCTGAGGTAgGAG
-----CtGcCCTGGctTTGctGtTCTCTTtAgGcGCTtCCAAgGtCCaGgGacAGGgG

TCTCGGGTGCCTGGGACCTACCAGGCACTCCATGCATCTCCATGGGGTCCCGACCCAGG
TCCTGGGcaGCTGGGACCTgCCAGGCCAtTcGTATCTCCATGGGGTCCaGACCCAGG
gtCTGGGCaCcaAGg--GctctGctAgGCTGTeCtYcagcCaCceCaCtGg

GACCCCACTTCTATCTGAGAGGACCAC-CCTTCTGAAGCTGGAACCTGATACTATT
GACCCCGTTCTcTATCTGAGAGGACCAC-TCTTCTGAAGCTGGAACCGATACTTgTT
GACCCtgcTCCcATCTGAGAGGACagCCcTCTTCTGgAGCTGGgAtCTGACcCTTgct

GTTGCCAAC---TGAACCAG EXON 1
GTTGCCAACcaCTGAACCAG
GTaCaAACGgcaaGATA



sites with increased binding had high stringency motifs, significantly fewer than the other 2 sets. Nevertheless, virtually all peaks had intermediate stringency matches consistent with ChIP-seq pull-down by HNF4 α antibody (Figure 3C). Analysis of other TF binding motifs showed clear differences between peaks with increased or decreased HNF4 α binding (Figure 3D). Peaks with increased HNF4 α binding showed enrichment of motifs from 5 reactive TF families that respond to injury and extrinsic signals (AP1, KLF, NF κ B, STAT, and ETS) and 2 hepatocyte-enriched families (CEBP and FOXA). AP1 (Jun-Fos family heterodimers) showed the most significant enrichment, followed by KLF and CEBP. Peaks with decreased HNF4 α binding showed depletion of the same motifs, especially CEBP. We explored the AP1 interaction further by analyzing the motif spacing in HNF4 α peaks where AP1 motifs were detected. The motifs were generally widely separated. Only 4% of AP1 motifs overlapped with HNF4 α motifs, and 87% were separated by more than 36 bp. AP1 and HNF4 α therefore bind separately, not at composite sites.

HNF4 α binding thus increased through cooperative interaction with other TFs that bind the same enhancer. Enhancers with decreased binding, exemplified by Peak 4 near the *Hnf4a-us* promoter (Figure 2A), had fewer additional TFs to facilitate binding and were thus sensitive to HNF4 α concentration.

Associating HNF4 α Binding With Altered Gene Expression

To analyze whether altered HNF4 α binding affected gene expression, ChIP-seq peaks were associated with the nearest active transcription start site within 50 kb (Supplementary Table 3), a conservative parameter, because enhancers that bind nuclear receptors like HNF4 α can be much more distant and can also regulate multiple genes.^{26,35} Peaks with increased and decreased binding of HNF4 α were then analyzed for correlation with changes in gene expression (Figure 4A). Up-regulated genes were enriched for peaks

with increased binding and depleted for peaks with decreased binding. Conversely, down-regulated genes were enriched for peaks with reduced binding and depleted for peaks with decreased binding. All correlations were significant but were much stronger for up-regulated genes.

To determine how these changes contributed to hepatocyte phenotype (Figure 4B and C), we compiled 2 correlating sets, up-regulated genes associated with increased and down-regulated genes associated with decreased total HNF4 α binding (Supplementary Tables 4 and 5). Although they do not include all regulations modified by the reduction in HNF4 α , these sets provided the clearest assessment of HNF4 α effects on gene expression. Genes in the up-regulated set individually increased far more than the average up-regulated gene and together comprised ~20% of the entire transcriptome. In contrast, genes in the down-regulated set showed weaker expression and were indistinguishable from other down-regulated genes.

Analysis for gene enrichment then significantly related each correlating set to gene profiles associated with liver decompensation. Up-regulated correlated set associations included cell death, cell survival, nuclear factor kappa B (NF κ B) signaling, stress, and fibrinolysis (Table 1). Down-regulated correlating set associations included general, lipid, mitochondrial, and bile acid metabolism (Table 2). (Note that HNF4 α -binding and correlating set genes are explicitly marked in Figures 5–7).

Gene Expression That Discriminates Decompensated Cirrhosis

Principal component analysis of RNA-seq libraries placed normal, CC14, and CC26 into widely separated groups (Figure 5A). The latter was most discriminated by remarkable expression of acute phase genes (Figure 5B), which indicated persistent inflammatory signaling 4 weeks after CCl₄ treatment had stopped. Most striking were *A2m* and *Serpine1*, 600- and 200-fold greater than normal liver, respectively, each 70-fold greater than CC14. In comparison,

Figure 2. (See previous page). *Hnf4a* isoform and lncRNA transcripts. (A) Comparison of HNF4 α promoter isoforms. The shorter P2 isoform lacked the N-terminal activation domain (A/B). (B) Comparative sequence of HNF4 α peak 4 (boxed region; Figure 1C), which encompassed the *Hnf4a-us* promoter and part of the first ncRNA exon. The conserved region (yellow) included a consensus promoter with TATA, INR, and 2 HNF4 α binding motifs. Despite high sequence conservation, an LXR motif was the only other significant ($P < 10^{-3}$) detection. The first exon, common to all isoforms in 3 species, diverged significantly and spliced to different nonhomologous regions in each species (compare normal rat and mouse liver in C). Most of the transcripts from this promoter were unspliced. (C) Transcript and splicing analysis of paired-end RNA-seq data. Sashimi plots show sense and antisense data in red and blue, respectively. Liver composite (top panel) shows *Hnf4a*-region transcripts compiled from all adult and fetal livers, normal or cirrhotic, in this article, with splices and transcript pileups. The detection frequency of each splice is marked above each intron. Data indicate 4 isoforms, P1 and P2 transcripts with alternate splicing of intron 10 (arrow). This was confirmed by analysis of exon reads (not shown). Antisense transcripts were present at much lower levels and showed variable splicing. Panels below show simplified plots (each compiled from 2–3 RNA-seq libraries) that display expression above minimum cutoff but not relative levels. Rat studies compare normal adult liver, 2 cirrhosis conditions, and 15-day fetal liver. Mouse studies compare normal liver and cholangiocytes. (D) PCR quantification of *Hnf4a* transcripts from mature rat and mouse liver. Both species had high levels of *Hnf4a* transcripts from promoter P1 and far less from P2. Both species also expressed lncRNAs from the –6 kb promoter, quantified by amplification across the first intron of rat *Hnf4a-us3* or mouse *Hnf4aos*. Nonspliced transcripts were amplified with the same exon primer and a primer from the adjacent intron. Note that RT-PCR was more sensitive than RNA-seq. (E) Rat transcript levels. Increased expression of *Hnf4a(P2)* did not compensate for loss of *Hnf4a(P1)* transcripts. Relative expression was calculated from exon 1 read levels and plotted as ratio to P1 isoform in whole liver. (F) Mouse transcript levels. Transcript levels are plotted as a fraction of the total hepatocyte or cholangiocyte transcriptome.

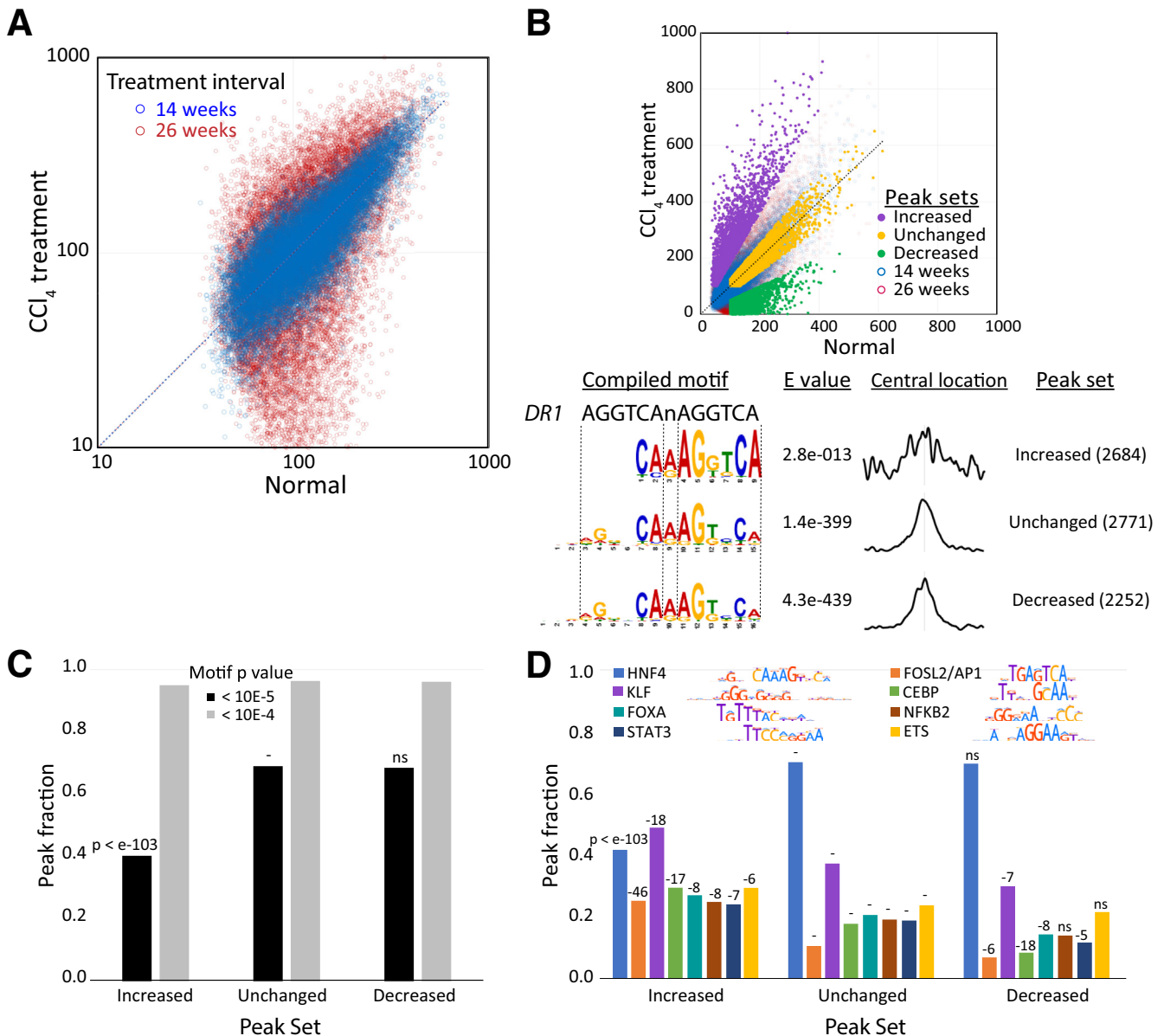


Figure 3. ChIP-seq analysis of HNF4 α binding. (A) Comparative binding of HNF4 α , showing overlay of 14- and 26-week binding data. The plot, 19,646 active sites that bound HNF4 α and H4K5Ac in any of the 3 experimental conditions, shows normalized peak areas (\log_{10}). Compilation, normalization, and filtering of the peak set are described in Materials and Methods. (B) Peak subsets and motif analysis. Three contiguous peak sets were selected: Increased (binding >1.7 -fold \times normal at 26 weeks); Decreased (binding <0.5 -fold \times normal at 26 weeks); and Unchanged (binding <1.25 - and >0.75 -fold \times normal). Set boundaries were selected to balance the number of peaks in each set. Early studies of strong binding sites showed that HNF4 α bound DNA as a head to tail dimer on a direct repeat of two 6-bp half sites separated by 1 bp (DR1), eg, the ideal 13-bp motif AGGTCA n AGGTCA.³² Motif discovery with *MEME-ChIP*, which calculates average binding sites from a group of sequences, gave nearly identical high-significance compilations of 13-bp motifs from both the Unchanged and Decreased peak sets. These closely reproduced compilations of HNF4 α binding sites^{20,26} and indicated that dimeric binding tolerates extensive variation in the first repeat, as well as central variation in the second repeat. Both compilations consisted of motifs within the centers of ChIP-seq peaks, as expected for pull-down with HNF4 α antibody. Compilation of the Increased peak set, in contrast, generated a related motif with much lower significance. This compilation showed even greater variation of the first repeat, although the second repeat was closer to the ideal motif. The compilation still consisted of motifs with central binding but over a wider range than the other 2 sets. (C) HNF4 α motifs (Increased, Decreased, and Unchanged from B). Peaks were scanned with the *FIMO* program using a reference HNF4 α motif compilation at stringencies for strong ($P < 10^{-5}$) and intermediate matches ($P < 10^{-4}$). At higher stringency, peaks with increased binding had significantly fewer motifs than both other groups. At intermediate stringency, virtually all peaks in each set showed HNF4 α motifs. *P* values, Fisher exact test vs control set with unchanged binding. (D) Peak scanning for other binding motifs. Using the *AME* program, significant correlations were detected to the HOCOMOCO motif set.³³ These were ranked by software-generated *P* values (vs the unchanged set). The motifs represent 2 groups, factors with increased expression in CC26 (FOSL2/AP1, KLF6, NF κ B, STAT3, and ETS); Figure 5) and phenotypic hepatocyte-enriched factors (CEBP, FOXA).

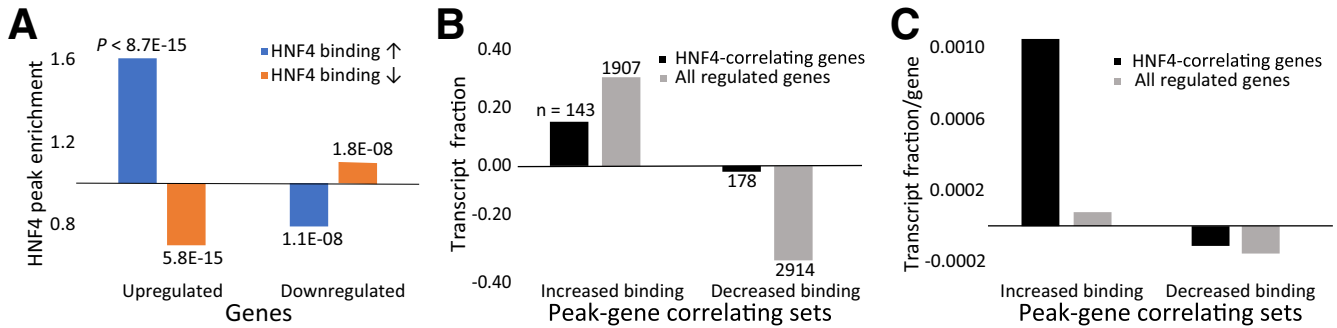


Figure 4. Correlation of HNF4 α binding with gene expression. (A) Relationship of altered HNF4 α binding to genes that change expression. The plot shows the correlation of HNF4 α peak binding (increased- and decreased-binding sets in Figure 2B) with associated up-regulated (>1.7-fold) or down-regulated (<0.59-fold) genes (Supplementary Table 3), plotted as the fraction of peaks in each set. P values, Fisher exact test. (B) Net transcription associated with increased and decreased HNF4 α binding. Gene expression was summed for sets of up-regulated genes associated with increased HNF4 α binding (143 genes, Supplementary Table 4) and down-regulated genes associated with decreased HNF4 α binding (178 genes, Supplementary Table 5). These were compared with the full sets of up- and down-regulated genes as fractions of the total transcriptome. (C) Transcription per gene. Data from B were divided by the number of genes in each set.

chronic treatment of rats with lipopolysaccharide, a common acute phase activator, caused only 14-fold increase of liver *A2m* mRNA.³⁶

Despite the increase in *A2m* transcripts, the absence of chromatin modification and TF binding was characteristic of a liver gene that is not expressed in hepatocytes (Figure 5C, left). This contrasts with the strong *A2M* expression of human hepatocytes. In contrast, *Serpine1* showed striking hepatocyte activation with new or increased binding of HNF4 α and CEBP β , increased H4K5Ac, and promoter H3K4Me3 (Figure 5C, right).

The acute phase phenotype was multicellular. *A2m* and *Vwf* were expressed in sinusoidal endothelium, *Orm1* and *Fgg* in hepatocytes, and *Lbp*, *Il1rn*, *Pla2g12a*, *App* in most liver cell types (Supplementary Table 7). *Serpine1* showed a remarkable transition, prominent expression in the stellate cells of normal liver, but de novo activation in cirrhotic hepatocytes.

The impact on hepatocyte-specific gene expression was also exceptional, affecting the most strongly expressed genes, all serum proteins (Figure 5D and E). Down-regulation of *Alb*, *Apoc1*, *Ttr*, *Apoe*, *Gc*, and *Ahsg* and up-regulation of *Serpina3n*, *Fga*, *Fgb*, *Fgg*, *Knk2*, *Hpx*, *Hp*, and *Orm1* remodeled the serum protein composition. Despite decreased *Hnf4a* expression, increased HNF4 α binding characterized most of these up-regulated genes.

Hepatocyte TF

In addition to the reduced expression of *Hnf4a*, CC26 greatly altered expression of nuclear receptor TF, particularly RXR and its heterodimeric partners (Figure 6). RXR closely relates to HNF4 α , which regulates the genes expressing RXR and most of their heterodimeric binding partners. Regulation is reciprocal, because several RXR heterodimers directly bind enhancers near *Hnf4a*. In addition, RXR heterodimers and HNF4 α bind similar motifs and frequently share the same enhancers.²⁶ Nuclear receptor

expression in CC14 was nearly normal, but CC26 showed depletion of *Rxra* and *Rxrg*; their partners *Nr1h3/LXR α* , *Nr1h4/FXR*, *Nr0b2/SHP*, *Nr1i3/CAR*, and *Thrb*; and circadian regulators *Nr1d1/REVERB α* and *Nr1d2/REVERB β* . However, the direct effect of reduced HNF4 α may be limited, because these genes all associated with HNF4 α binding sites, but only *Nr1h4* had a net reduction of HNF4 α binding (labeled green in Figure 7A; Supplementary Table 5).

The network of hepatocyte-enriched TFs has been enlarged here to include related hepatocyte TFs that bind common sequence motifs, often as heterodimers. Multiple TF classes are shown in Figure 7A and several types of leucine zipper (bZIP) TFs in Figure 7B. CC26 showed significant down-regulation of *Foxa1* and *Foxa2* but conserved expression of *Foxa3*. Metabolic TFs showed the greatest reductions, 90% for *Srebf1*, 60% for *Mxipl*, and 80% for the circadian PAR family (*Dbp*, *Hlf*, and *Tef*). Other reduced TFs, *Hhex*, *Gata4*, and *Zfp1*, encode mutually interacting developmental regulators that remain active in mature hepatocytes.^{37,38} Among these down-regulated genes, only *Foxa1* showed a net decrease of HNF4 α binding (Supplementary Table 5).

Expression of several major hepatocyte-enriched TFs was conserved. *Onecut1* and *Xbp1* showed consistent levels. In the larger CEBP and ATF-CREB groups, increased expression of *Cebpb* and *Atf4* suggest compensation of decreases in *Cebpa* and *Atf5*, respectively. Only the KLF family showed net up-regulation via strong induction of *Klf6*, a change associated with increased HNF4 α binding (Supplementary Table 4).

CC26 also induced widely expressed reactive TFs (Figure 7C). They are associated with signal transduction, injury, and inflammation, and most link to the acute phase response. Because multiple liver cell types express these factors, 2 criteria discriminated predominant hepatocyte expression, lack of depletion after hepatocyte isolation and H4K5Ac levels consistent with hepatocyte gene expression. CC26 induced 4 repressing TFs (*Atf3*, *Nfil3*, *Bhlhe40*,

Zbtb16), which could account for some of the observed transcriptional down-regulation. Each associated with HNF4 α -binding enhancers, and *Zbtb16* and *Bhlhe40* showed increased HNF4 α binding (Supplementary Table 4). However, stimulation of reactive transcriptional activators was more prominent. These included *Stat3*, NF κ B subunits (*Nfkb1*, *Nfkb2*, *Rela*), AP1 subunits (*Jun*, *Junb*, *Jund*, *Fos*, *Fosl2*), *Ets2*, and *Myc*.

STAT3 and NF κ B Responses

The most stimulated genes of CC26 were part of an acute phase response, which results from transcriptional activation by STAT3 and NF κ B. Activating TFs like these also reduces expression of some target genes, a potential mechanism for down-regulation of *Hnf4a*. To provide independent criteria for analyzing these responses, we used published RNA-seq and ChIP-seq data sets from mouse hepatocytes treated with interleukin IL1 and IL6³⁹ and compiled selective hepatocyte profiles, with common annotation in rat and mouse, of genes directly regulated by IL1-NF κ B or IL6-STAT3 (Figure 8A and B).

NF κ B responses were clear in CC14 but stronger in CC26, whereas STAT3 and combined responses discriminated CC26. The fold-change for STAT3 and NF κ B responders was similar, but the magnitude of STAT3

stimulation was much greater because it regulated strongly expressed transcripts (Figure 8C and D).

Comparison with 2 additional rat fibrosis models, BDL and TAA treatment, provided additional perspective (Figure 8E, Supplementary Table 6). Acute injury from treatment could be a significant cause of NF κ B and STAT3 activation, but the CC14 and CC26 and animals were held for 1 month following treatment before analysis. TAA and CCl₄ both cause similar centrilobular necrosis. The 6-month TAA livers had only 1 week of recovery, and acute injury was not fully resolved. Nevertheless, TAA livers showed the weakest responses, even the group with short recovery. BDL livers were studied without a recovery interval. They showed stronger NF κ B and STAT3 responses than CC14 but were still much less than CC26. The strongest responses were thus distinctive for CC26 and unrelated to acute injury. The reduction of HNF4 α was also distinctive for CC26, a correlation that led to further analysis of responses in mouse hepatocyte culture (Figure 8F).

Mouse primary culture data linked many CC26 changes in TF expression (Figure 9) to STAT3 and NF κ B signaling. Reactive TFs *Atf3*, *Fos*, *Stat3*, *Nfkb1*, *Nfkb2*, and *Junb* all showed clear binding by STAT3/NF κ B and strong induction by cytokine. *Myc*, *Ets2*, *Jun*, *Fosl2*, and *Klf6* already showed strong stimulation in control hepatocyte cultures, but cytokine treatment increased STAT3/NF κ B binding and gene expression.

Table 1. Gene Enrichment Analysis of the Up-regulated HNF4 α -correlated Set

Gene set	Overlap (n)	P value	Genes
GOBP REGULATION OF CELL DEATH (1814 genes)	39	9.1E-22	<i>Serpine1</i> , <i>Cdkn1b</i> , <i>Pim1</i> , <i>Mt1</i> , <i>Socs3</i> , <i>Sod2</i> , <i>Agt</i> , <i>Ncl</i> , <i>Lgmn</i> , <i>Bcl2l1</i> , <i>Dapk1</i> , <i>Rps6</i> , <i>Bnip3</i> , <i>Fga</i> , <i>Fgg</i> , <i>Fgb</i> , <i>Zfp36</i> , <i>Ddit4</i> , <i>Irak2</i> , <i>Fbxo32</i> , <i>Trp53inp1</i> , <i>Acer</i> , <i>Vhl</i> , <i>Bcl3</i> , <i>Btg2</i> , <i>Higd1a</i> , <i>Lgals3</i> , <i>Hcls1</i> , <i>Fgf21</i> , <i>Ramp2</i> , <i>Apbb3</i> , <i>Epcam</i> , <i>Gadd45b</i> , <i>Ccnl1</i> , <i>Cdc34</i> , <i>Gadd45g</i> , <i>Bcl2l11</i> , <i>Zbtb16</i> , <i>Usp36</i>
GOBP NEGATIVE REGULATION OF CELL DEATH (1143 genes)	26	4.0E-15	<i>Serpine1</i> , <i>Cdkn1b</i> , <i>Pim1</i> , <i>Mt1</i> , <i>Socs3</i> , <i>Sod2</i> , <i>Agt</i> , <i>Ncl</i> , <i>Lgmn</i> , <i>Bcl2l1</i> , <i>Dapk1</i> , <i>Rps6</i> , <i>Bnip3</i> , <i>Fga</i> , <i>Fgg</i> , <i>Fgb</i> , <i>Vhl</i> , <i>Bcl3</i> , <i>Btg2</i> , <i>Higd1a</i> , <i>Lgals3</i> , <i>Hcls1</i> , <i>Fgf21</i> , <i>Ramp2</i> , <i>Apbb3</i> , <i>Epcam</i>
HALLMARK TNFA SIGNALING VIA NF κ B (196 genes)	13	8.6E-14	<i>Serpine1</i> , <i>Socs3</i> , <i>Sod2</i> , <i>Zfp36</i> , <i>Bcl3</i> , <i>Btg2</i> , <i>Gadd45b</i> , <i>Ccnl1</i> , <i>Bhlhe40</i> , <i>Klf6</i> , <i>Pnrc1</i> , <i>Ninj1</i> , <i>Zbtb10</i>
GOBP NEGATIVE REGULATION OF STIMULUS RESPONSE (1722 genes)	27	7.2E-12	<i>Serpine1</i> , <i>Socs3</i> , <i>Sod2</i> , <i>Agt</i> , <i>Ncl</i> , <i>Lgmn</i> , <i>Bcl2l1</i> , <i>Fga</i> , <i>Fgg</i> , <i>Fgb</i> , <i>Zfp36</i> , <i>Ddit4</i> , <i>Vhl</i> , <i>Bcl3</i> , <i>Higd1a</i> , <i>Lgals3</i> , <i>Cdc34</i> , <i>Insig1</i> , <i>Lgals9</i> , <i>Dusp16</i> , <i>Spred2</i> , <i>Kng2</i> , <i>Ppp2ca</i> , <i>Csnkle</i> , <i>Ddx39b</i> , <i>Marveld3</i> , <i>Thbd</i>
GOBP REGULATION OF STRESS RESPONSE (1527 genes)	25	1.9E-11	<i>Serpine1</i> , <i>Socs3</i> , <i>Sod2</i> , <i>Agt</i> , <i>Bcl2l1</i> , <i>Fga</i> , <i>Fgg</i> , <i>Fgb</i> , <i>Zfp36</i> , <i>Irak2</i> , <i>Vhl</i> , <i>Gadd45b</i> , <i>Gadd45g</i> , <i>Insig1</i> , <i>Lbp</i> , <i>Lgals9</i> , <i>Ninj1</i> , <i>Dusp16</i> , <i>Spred2</i> , <i>Kng2</i> , <i>Ddx39b</i> , <i>Marveld3</i> , <i>Thbd</i> , <i>Spire</i> , <i>Ino80</i>
GOBP RESPONSE TO HORMONE (768 genes)	18	5.9E-11	<i>Socs3</i> , <i>Agt</i> , <i>Ncl</i> , <i>Rps6</i> , <i>Zfp36</i> , <i>Ddit4</i> , <i>Fbxo32</i> , <i>Hcls1</i> , <i>Ramp2</i> , <i>Trib3</i> , <i>Insig1</i> , <i>Eif4ebp1</i> , <i>Lepr</i> , <i>Cfl1</i> , <i>Slc39a14</i> , <i>Serpina3n</i> , <i>Alpl</i> , <i>Tat</i>
GOBP ENDOGENOUS STIMULUS RESPONSE (1725 genes)	25	2.5E-10	<i>Serpine1</i> , <i>Socs3</i> , <i>Agt</i> , <i>Ncl</i> , <i>Lgmn</i> , <i>Bcl2l1</i> , <i>Rps6</i> , <i>Zfp36</i> , <i>Ddit4</i> , <i>Fbxo32</i> , <i>Hcls1</i> , <i>Fgf21</i> , <i>Ramp2</i> , <i>Trib3</i> , <i>Insig1</i> , <i>Hnmpd</i> , <i>Eif4ebp1</i> , <i>Lepr</i> , <i>Cfl1</i> , <i>Slc39a14</i> , <i>Serpina3n</i> , <i>Alpl</i> , <i>Spred2</i> , <i>Tat</i> , <i>Got1</i>
HALLMARK MTORC1 SIGNALING (199 genes)	10	1.0E-09	<i>Lgmn</i> , <i>Ddit4</i> , <i>Btg2</i> , <i>Trib3</i> , <i>Insig1</i> , <i>Edem1</i> , <i>Bhlhe40</i> , <i>Aldoa</i> , <i>Got1</i> , <i>Stard4</i>
BIOCARTA FIBRINOLYSIS PATHWAY (11 genes)	4	3.3E-08	<i>Serpine1</i> , <i>Fga</i> , <i>Fgg</i> , <i>Fgb</i>
HALLMARK CHOLESTEROL HOMEOSTASIS (71 genes)	6	1.3E-07	<i>Lgmn</i> , <i>Trp53inp1</i> , <i>Lgals3</i> , <i>Trib3</i> , <i>Pnrc1</i> , <i>Stard4</i>

NOTE. Selected enrichment analysis (<http://www.gsea-msigdb.org>). 66/137 genes were identified in reference sets. Underlined genes were unique to a single set.

Table 2. Gene Enrichment Analysis of the Down-regulated HNF4 α -correlated Set

Gene set	Overlap (n)	P value	Genes
REACTOME METABOLISM (1769 genes)	42	6.7E-22	<u>Ugt2b37</u> , <u>Adh4</u> , <u>Cyp39a1</u> , <u>Ptgs1</u> , <u>Nr1h4</u> , <u>Ugt2b35</u> , <u>Acadsb</u> , <u>Hsd17b4</u> , <u>Acad10</u> , <u>Hao1</u> , <u>Adipor2</u> , <u>Sult1e1</u> , <u>Mgst2</u> , <u>Tkfc</u> , <u>Gcsh</u> , <u>Ddah1</u> , <u>Ppa2</u> , <u>Asrgl1</u> , <u>Adi1</u> , <u>Fech</u> , <u>Sptssa</u> , <u>Plaat1</u> , <u>Lrp2</u> , <u>Coasy</u> , <u>Nudt5</u> , <u>Mtmr4</u> , <u>Gsta1</u> , <u>Nat1</u> , <u>Tpst1</u> , <u>Suox</u> , <u>Ppox</u> , <u>Slc25a1</u> , <u>Pdp2</u> , <u>Hmox2</u> , <u>Psmf1</u> , <u>Oaz2</u> , <u>Hykk</u> , <u>Car3</u> , <u>Mocs1</u> , <u>Xylt2</u> , <u>Slc19a2</u> , <u>Plekha8</u>
GOBP SMALL MOLECULE METABOLIC PROCESS (1817 genes)	36	2.8E-16	<u>Ugt2b37</u> , <u>Adh4</u> , <u>Cyp39a1</u> , <u>Ptgs1</u> , <u>Nr1h4</u> , <u>Ugt2b35</u> , <u>Acadsb</u> , <u>Hsd17b4</u> , <u>Acad10</u> , <u>Hao1</u> , <u>Adipor2</u> , <u>Sult1e1</u> , <u>Mgst2</u> , <u>Tkfc</u> , <u>Gcsh</u> , <u>Ddah1</u> , <u>Ppa2</u> , <u>Asrgl1</u> , <u>Adi1</u> , <u>Fech</u> , <u>Sptssa</u> , <u>Plaat1</u> , <u>Lrp2</u> , <u>Coasy</u> , <u>Nudt5</u> , <u>Ces1f</u> , <u>Aldh8a1</u> , <u>Ptgr1</u> , <u>Angptl3</u> , <u>Wdtdc1</u> , <u>Mpc1</u> , <u>Gars</u> , <u>Aars2</u> , <u>Slc39a8</u> , <u>Pth1r</u> , <u>Fggy</u>
GOBP LIPID METABOLIC PROCESS (1450 genes)	27	9.8E-12	<u>Ugt2b37</u> , <u>Adh4</u> , <u>Cyp39a1</u> , <u>Ptgs1</u> , <u>Nr1h4</u> , <u>Ugt2b35</u> , <u>Acadsb</u> , <u>Hsd17b4</u> , <u>Acad10</u> , <u>Hao1</u> , <u>Adipor2</u> , <u>Sult1e1</u> , <u>Mgst2</u> , <u>Fech</u> , <u>Sptssa</u> , <u>Plaat1</u> , <u>Lrp2</u> , <u>Mtmr4</u> , <u>Ces1f</u> , <u>Aldh8a1</u> , <u>Ptgr1</u> , <u>Angptl3</u> , <u>Wdtdc1</u> , <u>Rab38</u> , <u>Pigc</u> , <u>Cd81</u> , <u>Slc16a11</u>
GOCC MITOCHONDRION (1838 genes)	28	1.3E-09	<u>Ugt2b37</u> , <u>Acadsb</u> , <u>Hsd17b4</u> , <u>Acad10</u> , <u>Gcsh</u> , <u>Ddah1</u> , <u>Ppa2</u> , <u>Fech</u> , <u>Coasy</u> , <u>Suox</u> , <u>Ppox</u> , <u>Slc25a1</u> , <u>Pdp2</u> , <u>Mpc1</u> , <u>Gars</u> , <u>Aars2</u> , <u>Rab38</u> , <u>Pxmp2</u> , <u>lfih1</u> , <u>Ung</u> , <u>Polrmt</u> , <u>Lig3</u> , <u>Pebp1</u> , <u>Armc1</u> , <u>Tufm</u> , <u>Tppp</u> , <u>Dnaja1</u> , <u>Tmem143</u>
REACTOME PHASE II CONJUGATION OF COMPOUNDS (102 genes)	7	1.4E-07	<u>Ugt2b37</u> , <u>Ugt2b35</u> , <u>Sult1e1</u> , <u>Mgst2</u> , <u>Gsta1</u> , <u>Nat1</u> , <u>Tpst1</u>
HALLMARK BILE ACID METABOLISM (111 genes)	7	2.5E-07	<u>Cyp39a1</u> , <u>Nr1h4</u> , <u>Hsd17b4</u> , <u>Hao1</u> , <u>Aldh8a1</u> , <u>Pxmp2</u> , <u>Slc29a1</u>
GOBP STEROID METABOLIC PROCESS (350 genes)	10	1.1E-06	<u>Ugt2b37</u> , <u>Cyp39a1</u> , <u>Nr1h4</u> , <u>Ugt2b35</u> , <u>Hsd17b4</u> , <u>Sult1e1</u> , <u>Fech</u> , <u>Lrp2</u> , <u>Ces1f</u> , <u>Angptl3</u>

NOTE. Selected enrichment analysis (<http://www.gsea-msigdb.org>). 69/163 genes were identified in reference sets. Genes unique to 1 set are underlined.

Hnf4a findings in hepatocyte culture were complex (Figure 9A–C). IL1-NF κ B induced down-regulation, but not IL6, although both cytokines down-regulated *Hnf4a*, the mouse upstream transcript (Figure 9B and C). Despite this inconsistency, other observations associated IL6-STAT3 with down-regulation of *Hnf4a*. First, IL6 increased STAT3 binding at *Hnf4a* enhancers, which also bound p65 (Figure 9A). Second, culturing alone substantially reduced *Hnf4a* without added IL6 treatment (Figure 9B). Finally, new analysis of hepatocyte cultures showed that cell isolation immediately induced a weak NF κ B response, and subsequent culturing induced progressive STAT3 and combined responses (Figure 9D), although the specific inducers of these responses are unknown. The cytokine treatments added to these prior responses. Seven additional TFs down-regulated in CC26 (*Rxra*, *Nr1h4*/FXR, *Hhex*, *Nr3c1*/GR, *Rara*, *Foxa2*, and *Mlxipl*) were also down-regulated by combined cytokine treatment in culture, with unambiguous local genomic binding of p65 or STAT3 (Figure 9E). Notably, *Nr1h4*/FXR was also part of the correlating subset with reduced binding of HNF4 α (Figure 6).

Changes in Nonparenchymal Cells

The NF κ B and STAT3 responses of hepatocytes arise from cell-extrinsic signaling. Potential sources were

determined from transcriptomes of hepatocytes, liver NPC, and inflammatory cell types. Because rat data were not available, RNA-seq libraries were compiled from mouse data, new stellate cell analysis, and published data sets from other cell types (Supplementary Table 7). Analysis defined sets of non-hepatocyte genes expressed in single cell types that could be distinguished in whole-liver RNA-seq data and then eliminated transcripts not detected in the rat experimental data (Supplementary Table 8).

In disease progression, changes in the levels of cell-specific transcripts could result from increased or decreased gene expression or a change in cell number. Transcripts that did not change expression would have near-median values in the distribution of expression changes. We used this property to compile cell-specific gene expression signatures (Figure 10A) for normalization of changes in all cirrhosis data sets (Supplementary Table 8). These signatures enabled quantification of cell populations during disease progression by measuring the fraction that each cell type contributed to the total liver transcriptome (Figure 10B and C).

CCl₄ injury increased most NPC types, although only stellate cells showed a much greater increase in CC26 (Figure 10B). However, BDL and TAA livers showed comparable levels of stellate cells (Figure 10C) and greater levels of cholangiocytes and Kupffer cells. TAA livers also

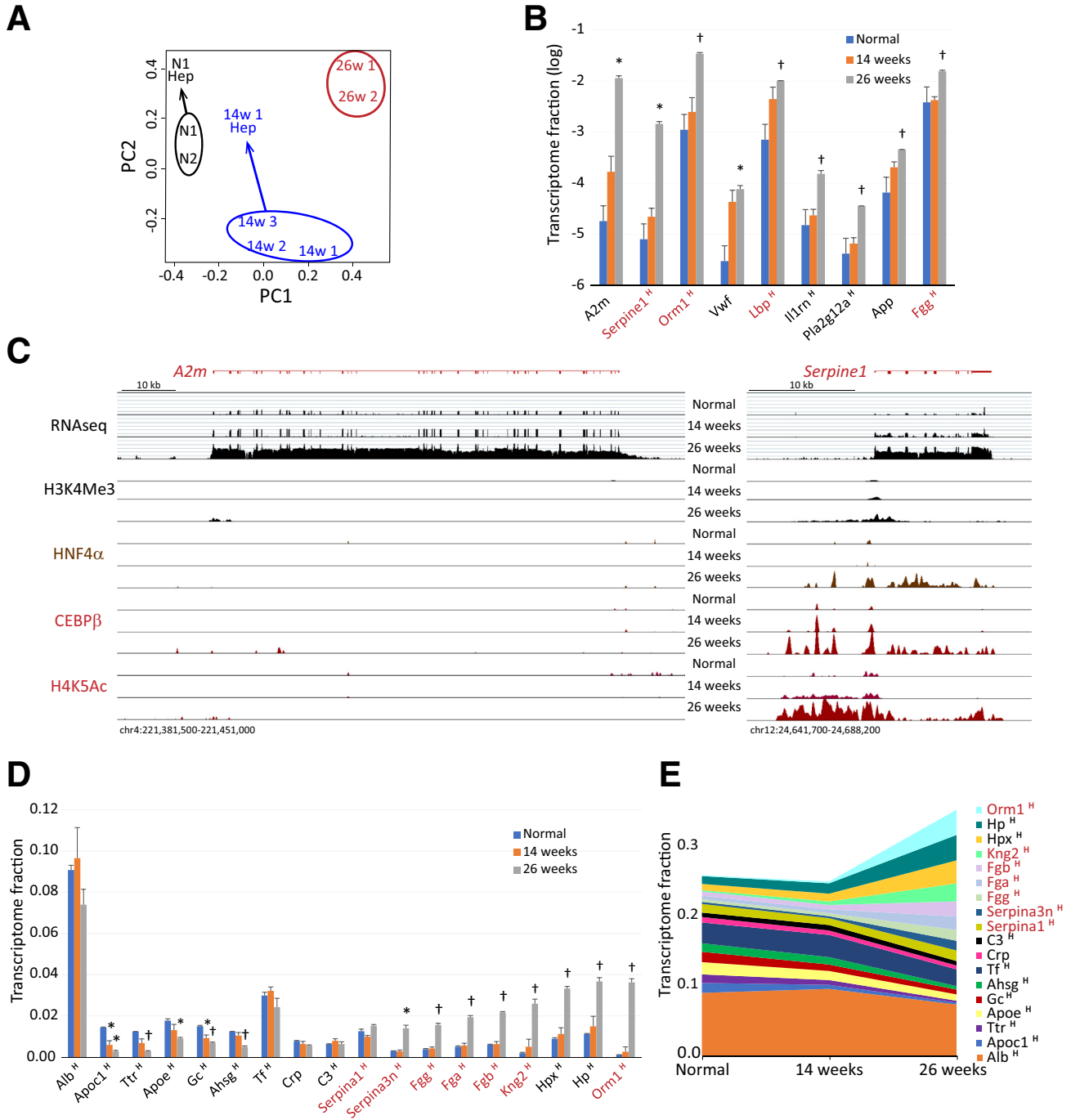


Figure 5. Discriminating transcriptional responses. (A) Principal component analysis of RNA-seq data sets separated the livers into 3 groups. Comparison with isolated hepatocytes (hep) from 2 livers showed that much of the group separation resulted from changes in nonparenchymal cells. (B) The most stimulated transcripts all encoded acute phase proteins. (C) Genomic views of liver *A2m* and *Serpine1*. See Figure 1A description. (D) Expression of most abundant hepatocyte transcripts. All encoded serum proteins. They are inversely ranked by the incremental transcriptional change in 26-week cirrhosis. (E) Pileup of serum protein transcript levels. The massive acute phase response markedly changed the serum protein composition. In B, D, and E, gene names marked with “H” indicate association with HNF4 α binding sites (Supplementary Table 3); red indicates increased total binding of associated HNF4 α (Supplementary Table 4). Quantification is presented as fraction of total transcripts. *t* tests, *P* vs normal liver, * $<.05$, † $<.01$.

showed higher levels of fibroblasts. Infiltrating inflammatory cells, especially macrophages and neutrophils, will reflect direct tissue injury and are potential sources of

STAT3 and NF κ B activation. However, levels of inflammatory cells levels did not discriminate CC26 from other groups. The functional decompensation of CC26 did not

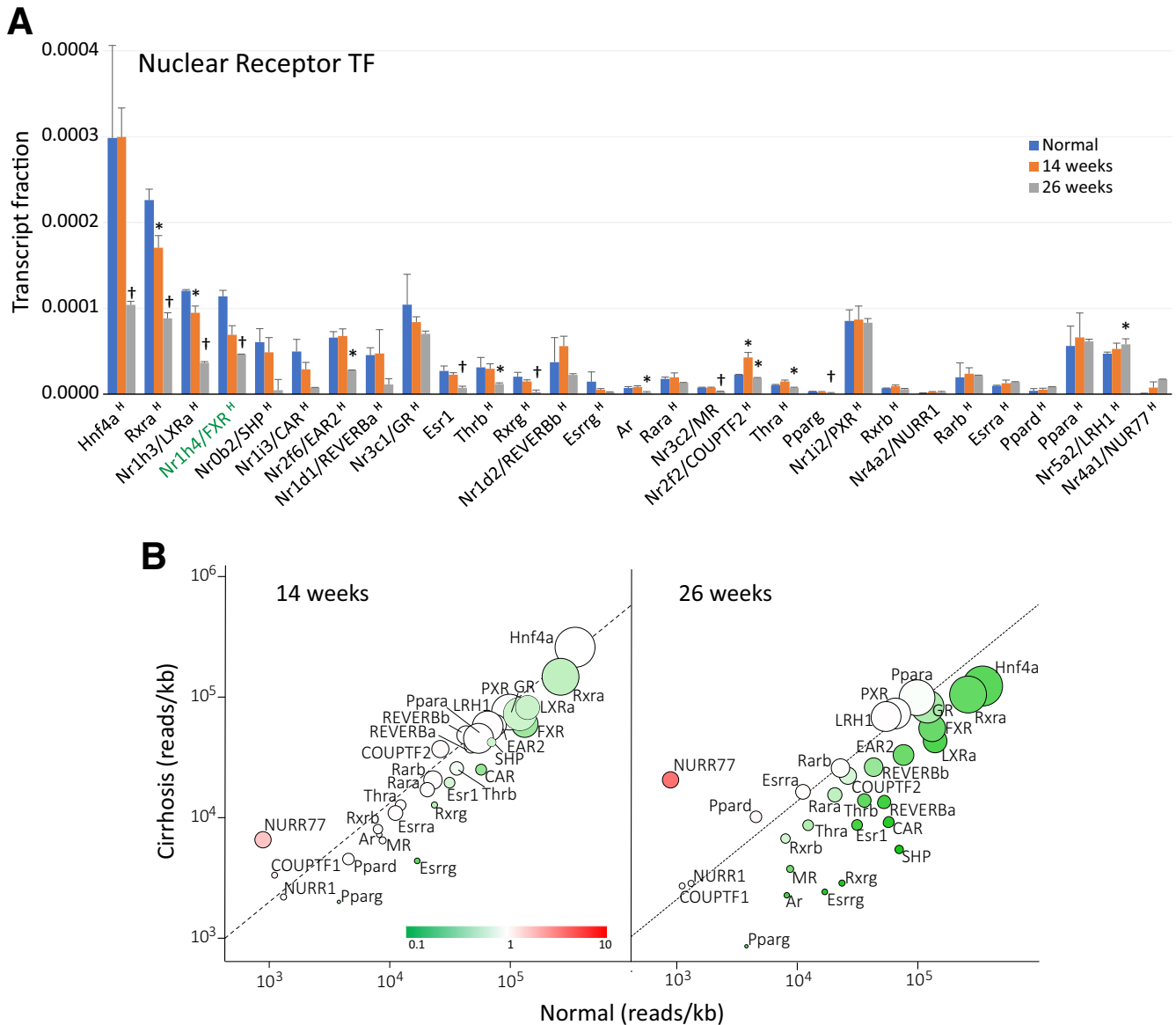


Figure 6. Progressive changes in expression of nuclear receptor TF. (A) The 29 hepatocyte-expressed nuclear receptors are displayed, labeled by gene symbols and common names. Gene names marked with “H” were associated with HNF4 α binding sites (Supplementary Table 3); green indicates decreased total binding of associated HNF4 α (Supplementary Table 5). (B) Bubble plots comparing 14- and 26-week cirrhosis demonstrate the broad loss of expression in decompensated cirrhosis.

therefore evolve directly from progressive liver damage or inflammation.

NPC also responded to NF κ B/STAT3 signaling in CC26. Stellate cells showed the most NF κ B responders, whereas STAT3 responders distributed more broadly (Figure 10D and E, Supplementary Table 8).

Cell Type Expression of Acute Phase Cytokines and Receptors

RNA-seq detected expression of 17 cytokines that can activate NF κ B or STAT3 (Figure 11A and B), potential mediators of decompensation. Their likely cells of origin were determined with the mouse cell-type library resource

(Supplementary Table 7). Two NF κ B activators (*Il1b* and *Tnf*) increased in CC26, mostly *Il1b*, expressed by sinusoidal endothelium⁴⁰ or Kupffer cells.

Four STAT3 activators (*Il6*, *Osm*, *Clcf1*, *Il10*) were elevated in CC26. *Osm* increase was greatest and most selective. Endothelial cells were the most abundant source in normal liver, although increases in macrophages and neutrophils made these cells possible secondary sources in CC26. Regardless, the calculated cell proportions indicated that *Osm* expression reflected a higher level of transcription and not just an increase in an expressing cell type. In contrast, the levels of cholangiocyte-specific *Clcf1* paralleled the increased cholangiocytes observed in all models, a passive change (Supplementary Table 8).

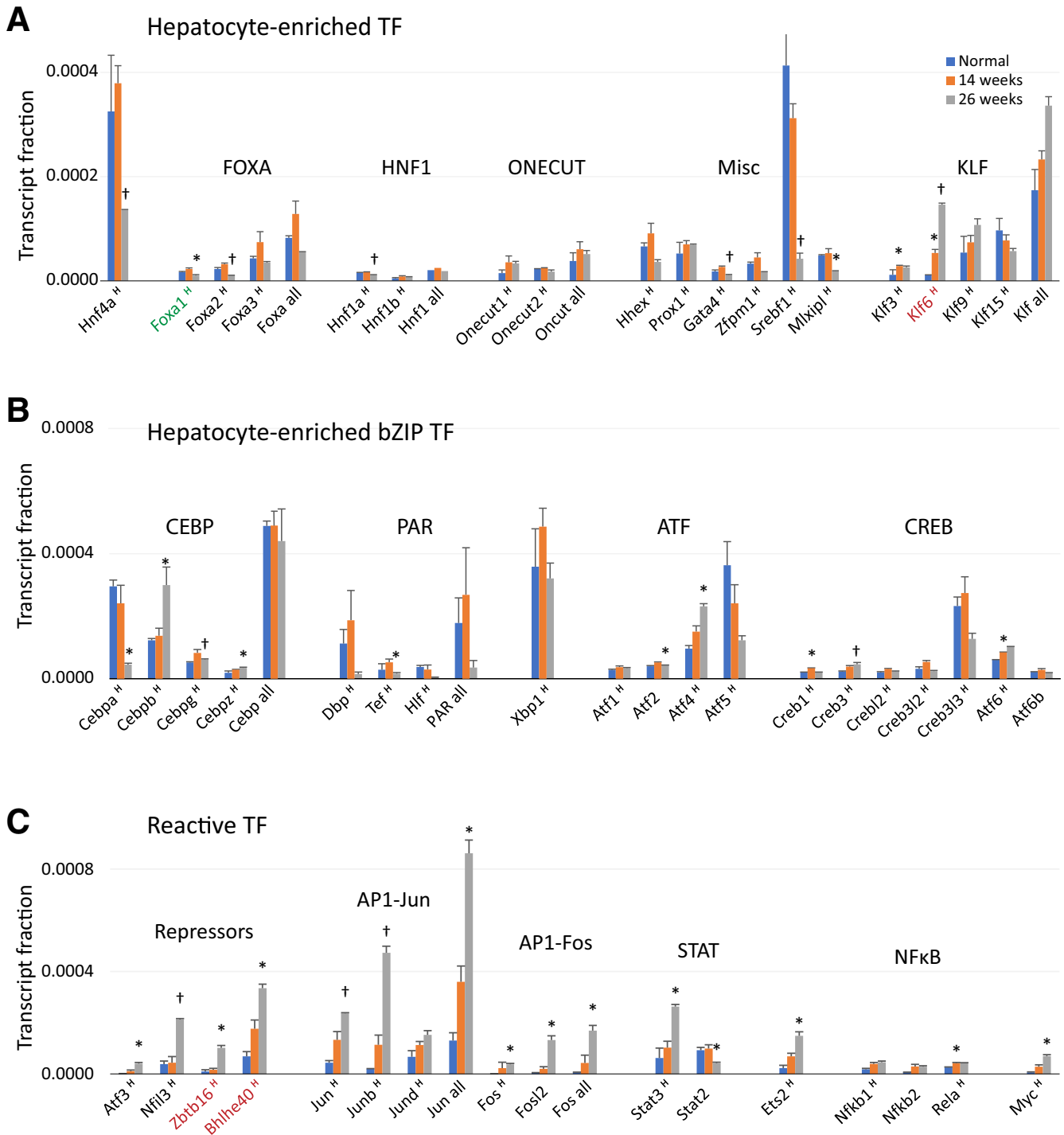


Figure 7. Hepatocyte-enriched and reactive TFs. (A and B) Full network of hepatocyte-enriched TFs, grouped as families with common DNA binding. Because they share in regulation, all hepatocyte-expressed family members are shown if one is hepatocyte enriched. The plots also show the sum of transcripts for several families with common binding sites: FOXA, HNF1, ONECUT, KLF, CEBP, and PAR. (C) Reactive TFs. Except for the AP1 FOS and JUN families, the plot shows TFs that have changed expression 2-fold after 14 or 26 weeks. Four repressing TFs are grouped on the left. Reactive *Nr4a1/NUR77* is displayed with nuclear receptors in Figure 6. A. The plots show mean, standard deviation and *t* tests compared with normal liver: * $P < .05$; † $P < .01$. Gene names marked with “H” were associated with HNF4 α binding sites (Supplementary Table 3); red indicates increased and green indicates decreased total binding of associated HNF4 α (Supplementary Tables 4 and 5).

Normal hepatocytes expressed *Il6r* and *Lifr*; the CLCF1 receptor, but not *Osmr* (Figure 11C and D). However, strong hepatocyte expression of *Osmr* appeared in CC26 along with

progressive de-repression and activation of chromatin (Figure 12A). This is consistent with analysis of cultured hepatocytes, which showed that IL1 and IL6 additively

stimulated *Osmr* expression and induced binding of NF κ B-p65 and STAT3 near the promoter (Figure 12B and C).

The multicellular integration of the decompensation in CC26 is summarized in Figure 13. It resulted from unusually strong NF κ B and STAT signaling. NPCs were both targets and sources of activating cytokines, whereas hepatocytes were exclusively targets.

Discussion

Acute phase signals primarily impact hepatocyte transcriptional regulation by inducing new activating TFs, but such activators can also act as transcriptional inhibitors. TFs act through networks of mutual regulation, so inhibiting central regulators like HNF4 α has broad effects. The following discussion will consider the regulation of transcripts encoded within *Hnf4a*, the impact of reduced HNF4 α on gene expression, and how activating TFs may inhibit gene expression. The discussion will then return to cell integration to consider the pathogenesis of liver decompensation.

HNF4 α Isoforms

HNF4 α was first characterized in liver^{41,42} as a master regulator development and the mature phenotype. Within the liver, our analysis demonstrated only 4 HNF4 α isoform transcripts, exon 10 splice isoforms α 1 and α 2 from P1 and corresponding isoforms α 7 and α 8 from P2.^{43,44} Both promoters are active in fetal liver. In mature liver, only P1 is active, although P2 transcripts were still detectable by RT-PCR, 0.03% of total *Hnf4a* transcripts, below the threshold of RNA-seq detection. The wide separation of P1 and P2 may partition the 2 promoters into separate transcription activation domains, but P2 is still less than 30 kb from the upstream enhancer cluster and does not respond to it. Instead, P2 shows repression (H3K27Me3) typical of a non-hepatocyte promoter.

P1 and P2 encode similar forms of HNF1 α , but the absence of the A/B domain in P2 isoforms indicates loss of one type of transcriptional activation. Thus, mice engineered to express the P2 isoform from both promoters show normal liver development but have altered lipid metabolism and stress responses.^{44,45}

P2 transcripts were significantly increased 85-fold in CC26 compared with normal liver (Figure 1B). Increased P2 transcripts were also observed in decompensation of human alcohol-associated liver disease.²³ Nevertheless, in our model, the increase amounted to a small fraction of total *Hnf4a* transcripts. The P2 promoter and upstream regions showed new TF binding and activation markers, also at low levels. These small changes suggest that the new expression came from another cell type, not hepatocytes. A precedent study of *Hnf4a* in colon demonstrated that the P1 and P2 promoters functioned in transcriptional regulatory environments of different crypt cell types.⁴⁶

Comparison of non-hepatocyte transcriptomes from liver (Supplementary Table 7) showed strong *Cebpb* expression in most cell types, but *Hnf4a* expression was observed only in cholangiocytes. The weak ChIP-seq detections (arrows in

Figure 1A) of CEBP β , HNF4 α , H3K4Me3, and H4K5Ac could therefore represent cholangiocyte expression, which selectively expressed P2 transcripts (Figure 2C). It should be noted that the Sashimi plots in Figure 2 directly visualize unprocessed sequence reads and provide unbiased quantification of entire transcripts. Compilations of read pileups over exons further confirmed the splicing quantifications. Selective expression of *Hnf4a(P2)* in cholangiocytes was previously detected with isoform-specific antibodies.^{30,31} Fetal liver, which was included as a positive control, expressed the highest levels of P2 isoforms, but P1 expression was still dominant (Figure 2D and E), consistent with the quantifications of Briançon et al.²⁷ Their study also characterized a 4-kb P2 “promoter” and showed control by *Onecut1/HNF6* and *Onecut2*, which are predominantly cholangiocyte TFs (Supplementary Table 7). Moreover, this 4-kb segment directed transgenic reporter gene expression in fetal stomach, intestine, and pancreas, but not liver.²⁷

Thus *Hnf4a(P1)*, controlled by extensive regions of highly active enhancers, dominates liver development, mature liver, and disease progression. Increases in *Hnf4a(P2)* expression significantly mark disease progression but probably reflect non-transcriptional mechanisms that increase the number of cholangiocytes.

Upstream Transcripts

The *Hnf4a* region has a third promoter at -6 kb that initiates antisense lncRNA transcripts. At this distance, it is clearly an independent promoter, with a broad strong H3K4Me3 peak that indicates a high level of activity. *Hnf4a(P1)* and *Hnf4a-us* promoters apparently compete for nearby enhancers to stimulate transcription. Several attributes indicate the importance of *Hnf4a-us*: promoter strength, similar lncRNA genes in mouse and human, high promoter region sequence conservation greater than P1 or P2, and coregulation of *Hnf4a-us* and *Hnf4a(P1)* transcription.

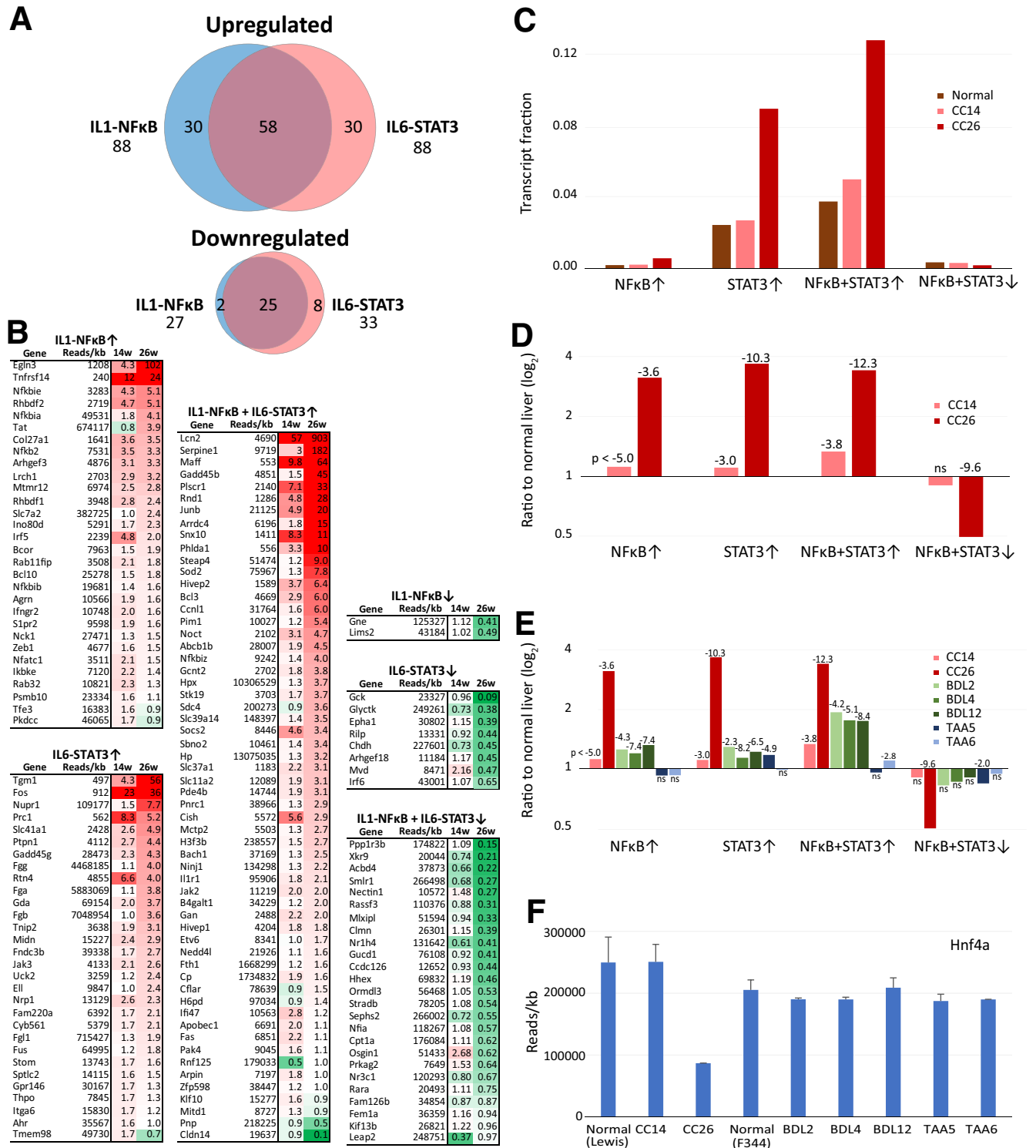
The lncRNA transcripts comprise multiple spliced isoforms, but the visualizations and quantifications (Figures 1A and C and 2D) demonstrated that most transcripts were unspliced. The transcripts covered the entire upstream enhancer region and showed a striking down-regulation in CC26, a change that paralleled chromatin acetylation (H4K5Ac) and *Hnf4a(P1)* gene transcription. The unusually high level of unprocessed transcripts suggests a high transcription rate and rapid turnover (compared with the more typical ~1% unprocessed transcript level from *Hnf4a(P1)*). Repeated transcription through the region might affect activation, looping, unlooping, or queuing of individual enhancers for interaction with the *Hnf4a(P2)* promoter. The *Hnf4a-us* lncRNAs are distinct from eRNA, which are short local transcripts that stimulate enhancer function by stabilizing loops and coactivating catalytic histone acetylation by CBP.⁴⁷ eRNA are too short for detection by RNA-seq, but fragments of longer lncRNAs might have similar function.

The processed lncRNA might have a specific transcriptional or non-transcriptional function,⁴⁸⁻⁵⁰ presumably

through the first exon, the only region common to rat, mouse, and human transcripts (Figure 2B). The low transcript level (~7 molecules/cell) implies few regulatory targets, which is consistent with a recent study of the human homolog, *HNF4AS1*, that suggested direct

lncRNA regulation of TF binding near the *Hnf4a(P1)* promoter.⁵¹

Additional observations suggest an intriguing relationship between HNF4 α concentration and control of *Hnf4a(P1)* gene expression. There are 10 above-threshold



HNF4 α peaks in the upstream and downstream regulatory regions. Average binding at these peaks showed a slight increase (11%) in CC26. Paradoxically, Peak 4, which encompasses the highly conserved transcription controls of *Hnf4a-us*, showed total loss of HNF4 α binding (Figure 1C). Like other HNF4 α sites that lost binding in CC26, in silico analysis failed to show supporting TF-binding motifs in Peak 4. Transcription of *Hnf4-us* apparently depends on this critical weak binding site and is therefore directly sensitive to the concentration of HNF4 α . *Hnf4a-us* transcription apparently acts as a brake that helps maintain a constant level of *Hnf4a(P1)* transcription. Thus, normal *Hnf4a-us* transcription slows increases, whereas reduced *Hnf4a-us* transcription slows decreases of HNF4 α concentration.

Mechanism of Altered HNF4 α Binding

Despite its reduced expression in CC26, HNF4 α binding decreased at only a fraction of enhancers. Although low-affinity sites would be expected to have greatest sensitivity to HNF4 α concentration, enhancers that lost binding had a motif distribution that was identical to sites that did not change binding. The reduced binding instead exemplified fundamental properties of enhancers, which function through “integration of several weaker interactions”⁵² via “cooperative assembly and stability” of a TF complex.⁵³ Cooperativity arises from the highly organized assembly that optimally aligns the TFs to interact with DNA, coactivators, mediator, and general TFs. The paucity of other TF motifs suggests that fewer cooperative partners, not DNA binding affinity, reduced HNF4 α binding by these enhancers.

Cooperative interactions can also explain the increased HNF4 α binding at activated enhancers, despite low-affinity binding sites. These enhancers showed enrichment of motifs for reactive TF induced in CC26, especially AP1 (JUN: FOS) heterodimers. Consistent with these observations, common binding of HNF4 α and FOSL1 was demonstrated at some enhancers in HC116 cells, as well as direct binding of HNF4 α to FOSL1 in vitro.⁵⁴ Our motif analysis showed that AP1 and HNF4 α binding sites were mostly in different parts of these enhancers, which is still consistent with co-recruitment by mutual affinity. These AP1 relationships also suggest a second mechanism for increased binding, exemplified by interaction with a similar TF, the

glucocorticoid receptor (*Nr3c1*). In this case prior AP1 binding opened the chromatin and preprogrammed the enhancer for subsequent nuclear receptor binding.⁵⁵ Both cooperation and preprogramming to stimulate HNF4 α binding may also apply to other reactive TFs in CC26.

Mechanism of Reduced HNF4 α Expression and Other Transcriptional Changes

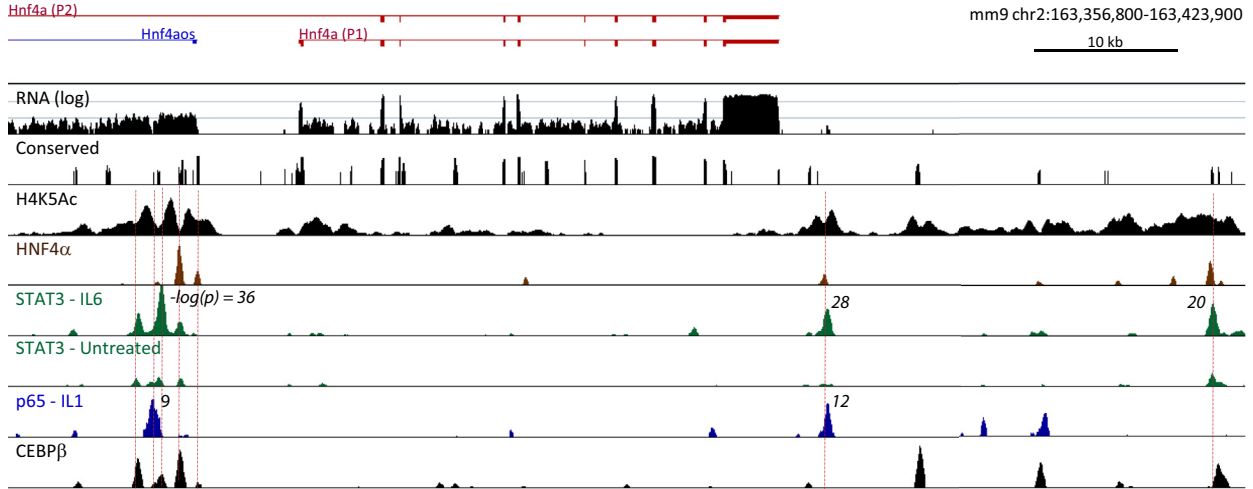
HNF4 α autoregulates *Hnf4a* and activates hepatocyte TF genes that comprise a network of mutual regulation. Down-regulation of *Hnf4a* might therefore synergistically attenuate expression of network TFs. However, network synergy does not explain the critical process that initially down-regulated *Hnf4a*. We therefore investigated the acute phase response, the most striking feature of the CC26 phenotype, to explain the down-regulation.

All cirrhotic livers showed direct transcriptional responses characteristic of NF κ B or STAT3 activation. However, CC26 showed the strongest positive responses and was the only condition that showed negative responses, which apparently required higher levels of STAT3 and NF κ B. Many stimulatory TFs also inhibit transcription of some target genes. Such inhibition may occur via competition between TF. Alternatively, epistatic interactions can alter the local shape of the DNA, chromatin accessibility, or nucleosome conformation and can inhibit binding of other TFs.⁵⁶ The requirement for high levels of NF κ B-p65 or activated STAT3 suggests concentration-dependent effects, such as binding at low-affinity sites or competition with other TFs that normally assemble on the enhancer.

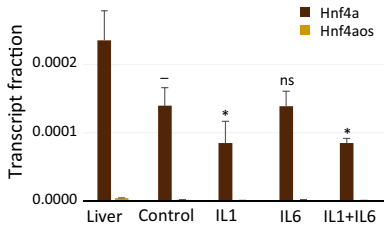
Expression of multiple TFs showed clear direct inhibition by IL1-NF κ B or IL6-STAT3 in hepatocyte culture, but *Hnf4a* inhibition was only partially consistent. IL1 treatment strongly reduced expression and induced p65 binding to multiple *Hnf4a* enhancers. IL6 treatment increased binding of STAT3 but did not decrease gene expression. However, cultured hepatocytes already had lower *Hnf4a* expression than liver in vivo. This reduction could have resulted from the prior activation of STAT3 that occurs in cell culture or another equivalent inhibitory mechanism. It reflects a limit of primary culture studies because hepatocyte phenotype and responses often deviate from liver in vivo.

Figure 8. (See previous page). NF κ B and STAT3 signaling. (A) Hepatocyte genes that directly respond to NF κ B and STAT3. Discriminating sets of responsive genes with unambiguous hepatocyte expression, either up- or down-regulated, were defined by analysis of RNA-seq and ChIP-seq libraries from mouse hepatocytes treated with IL1 or IL6.³⁹ Selected genes showed cytokine-induced transcriptional changes accompanied by binding of NF κ B-p65, STAT3, or both. Up-regulation and down-regulation were cut off at >1.7 and $<0.65 \times$ control, respectively. Single-effect genes bound NF κ B-p65 for IL1 or STAT3 for IL6 and responded to one cytokine. Dual responders showed additive or synergistic stimulation and bound both TFs, often at different enhancers. Profiles were limited to genes with common annotation in mouse and rat. Mouse profiles were then used to analyze rat responses. (B) NF κ B and STAT3 response profiles in CCl₄-induced cirrhosis. Gene profiles, overlaid with heat maps, are listed with expression changes in cirrhosis. Data columns: expression in normal liver (reads/kb) and fold-change after 14 and 26 weeks of treatment. (C) Expression of NF κ B and STAT3 responses. The plot displays the summed expression of genes in each response profile as a fraction of total transcripts. STAT3 responders were expressed at much higher levels than NF κ B responders. (D) Average changes in gene expression. Fold-change was averaged for the genes in each profile. *P* values for enrichment of profile genes were calculated with Fisher exact test. (E) Comparison with other fibrosis/cirrhosis models. Data from C are compared with BDL and TAA-induced cirrhosis. (F) Comparison of *Hnf4a* expression in the liver injury models. Control normal liver: Lewis rats for CCl₄ treatment, F344 rats for BDL and TAA treatment.

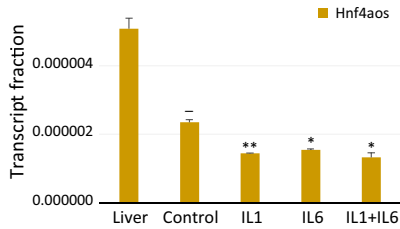
A



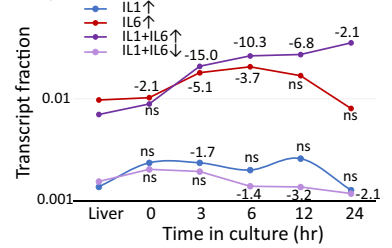
B



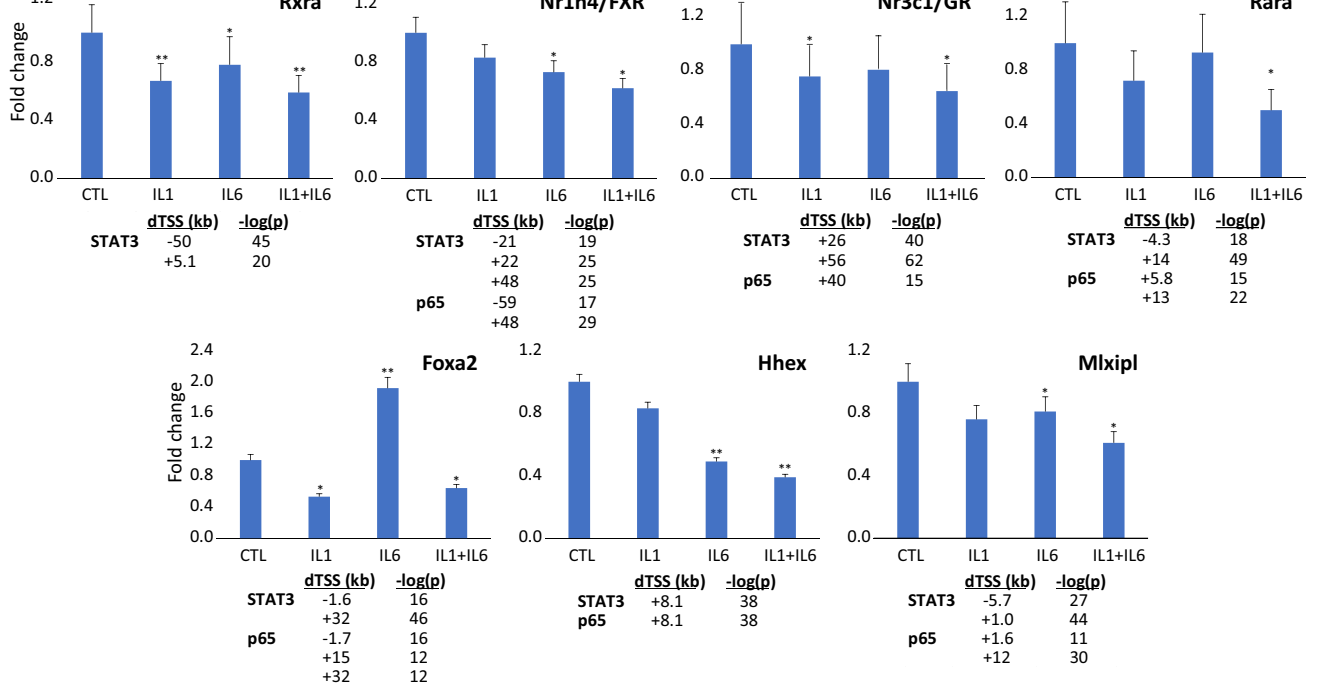
C



D



E



Impact of Reduced HNF4 α

Hnf4a down-regulation was prominent in a process that also reduced expression of other TFs. However, it is not clear whether the reduced level of HNF4 α was critical because mice with liver-specific heterozygous knockout, a comparable loss of expression, were phenotypically normal.⁵⁷ Down-regulation directly associated only with moderate expression changes, and there was still enough HNF4 α to markedly increase binding and contribute to the high level expression of phenotypic genes. Such down-regulation could be adaptive by allowing reprioritization of transcriptional resources for compensation of tissue injury. Nevertheless, HNF4 α did associate with important hepatocyte processes that are altered in cirrhosis and decompensation (Table 2). Some of these down-regulations could have critical effects that might be reversed by therapeutic supplementation of HNF4 α .^{19,21,22}

Integration of Cellular Responses

Our CCl₄ treatment model produced decompensation of hepatic function with clinical signs of end-stage liver disease (eg, ascites, encephalopathy, coagulopathy) at least 4 weeks after the animals had completed CCl₄ treatment, when we began our analysis. The TAA fibrosis and BDL models did not produce end-stage disease, although cell populations that reflected progression of cirrhosis and inflammation had comparable or greater increases than in CC26.

BDL damages both cholangiocytes and hepatocytes, the latter through bile acid accumulation, sterile inflammation, and hepatocyte apoptosis.⁵⁸ There is also loss of bile duct integrity with formation of bile lakes. The BDL rats were studied at the time of maximum damage without a recovery interval and showed significant STAT3/NF κ B responses, although much weaker than CC26.

Chronic TAA injury is often considered a more effective model of progressive cirrhosis than CCl₄ injury. Like CCl₄, TAA induces centrilobular hepatic necrosis with infiltration by inflammatory cells as the acute injury resolves,⁵⁹ considerably more direct hepatocyte damage than BDL. Compared with CC26, TAA showed more fibroblasts and cholangiocytes that reflected greater tissue damage during disease progression. There were also more Kupffer cells, macrophages, and neutrophils, especially at 6 months,

reflecting active tissue damage. At the time of tissue sampling after a nontreatment recovery interval, STAT3 and NF κ B signaling were low, although they were likely higher shortly after TAA administration.

The distinctive CC26 phenotype indicated persistent inflammatory signaling, although the interval after the last CCl₄ treatment was long enough to totally resolve the acute injury and inflammation from this toxic agent. The persistent signaling therefore indicates a second process superimposed on progressive cirrhosis. This process is comparable with acute-on-chronic decompensation of cirrhosis observed in some human patients, which is also associated with acute phase proteins and inflammatory mediators. Analysis has associated this human liver pathogenesis to extrinsic systemic inflammation originating from the gut, with progression from bacterial overgrowth to bacteremia.^{60,61}

Experimental models induce an acute phase response by treatment with either turpentine or bacterial lipopolysaccharide. Both elevate circulating cytokines and stimulate the liver to synthesize acute phase proteins. *I11b* expression reveals a critical difference between the 2 treatments.⁶² Peripheral injection of turpentine induced local inflammation that released IL1 β (and IL6), which remotely stimulated but did not damage the liver or activate hepatic transcription of *I11b*. Thus, cytokine stimulation alone was not sufficient to activate cytokine gene expression within the liver. In contrast, intraperitoneal injection of lipopolysaccharide induced the liver to transcribe *I11b*, part of a more complex systemic inflammatory response. Similarly, endotoxin induced liver *Osm*, but turpentine did not.^{63,64} The liver of CC26 therefore showed inflammatory signaling that can be experimentally induced by endotoxin, which acts through toll-like receptor 4. Other toll-like receptor activators, such as viral components, might also induce similar responses. These are important possibilities, but it must be emphasized that our study, which is confined to liver specimens and genomic transcription, did not define the specific mechanism of chronic STAT3/NF κ B activation in CC26.

Despite this limitation, the analysis provided important information about the multicellular pathogenesis. The decompensation of CC26 resulted from complex interactions among NPC and hepatocytes. Both hepatocytes and

Figure 9. (See previous page). *Hnf4a* responses to cytokine in cultured mouse hepatocytes. (A) ChIP-seq analysis of mouse *Hnf4a*. Promoters and enhancers of mouse and rat *Hnf4a* are highly conserved (compare with Figure 1C). NF κ B-p65 and STAT3 ChIP-seq data from cultured hepatocytes (Goldstein et al)³⁹ are displayed with reference ChIP-seq compilations of HNF4 α , CEBP β , and H4K5Ac from normal liver²⁶ and a track showing mammalian sequence conservation (phastCons30way). Multiple p65 and STAT3 peaks localize to enhancers where H4K5AC is locally depleted (red lines), along with HNF4 α and CEBP β . STAT3 binding was present in untreated cultures but increased with IL6 treatment. Detection significance, $-\log(p)$, is listed next to major STAT3 and p65 peaks. (B and C) *Hnf4a* and *Hnf4aos* transcription. Hepatocytes were cultured for 22 hours in Dulbecco modified Eagle medium and treated with cytokine IL1 and IL6 for 2 hours (data sets from Goldstein et al).³⁹ *Hnf4aos* is the mouse upstream antisense transcript homologous to rat *Hnf4a-us3* (Figure 2). Plots show mean, standard deviation, and *t* tests of RNA-seq data compared with the cell culture control and normal liver. (D) Sequential hepatocyte responses in culture. Hepatocytes were isolated, cultured in Dulbecco modified Eagle medium, and sampled at multiple intervals. Curves show total expression of profile genes, plotted on a log₁₀ scale as a fraction of the total transcriptome. Note that dual IL1 + IL6 responses were persistent at 24 hours. *P* values vs normal liver, displayed with the data points, were calculated with Fisher exact test. (E) Additional TFs inhibited by cytokine. These genes showed <65% of control transcripts after combined IL1 + IL6 treatment. Significant STAT3 or p65 binding peaks within 60 kb are listed with distance from the transcription start site, dTSS, and significance of peak detection, $-\log(p)$.

endothelial cells produced extreme levels of acute phase proteins. The main activating cytokines were OSM and IL1 β , produced by endothelium, Kupffer cells, or macrophages. The main target cells for the response, which were hepatocytes, endothelium, and stellate cells, all expressed the necessary receptors, but OSM responsiveness was a special adaptation. Silent in normal hepatocytes, the additive contributions of NF κ B and STAT3 activated *Osmr* expression to progressively amplify the inflammatory signals. The strong NF κ B and STAT3 signaling profoundly altered the hepatocyte phenotype, inducing acute phase proteins, simultaneously reducing expression of HNF4 α and TFs that dynamically regulate metabolism.

Materials and Methods

Animals

Lewis rats and C57Bl/6 mice were maintained in isolation cages in the Department of Laboratory and Animal Resources at the University of Pittsburgh. Animals were housed in temperature- and light/dark cycle-controlled rooms. All animal experiments were approved by the Institutional Animal Care and Use Committee at the University of Pittsburgh.

Induction of Cirrhosis

Liver cirrhosis was induced in rats as described in Nishikawa et al,¹⁹ which provides a detailed treatment description. The current studies were carried out on livers from some newly treated rats and frozen liver specimens archived from this prior study. Briefly, 4-week-old male rats were given phenobarbital (0.5 g/L) in drinking water. Two weeks later, CCl₄ was administered by biweekly gavage at 0.2 mL/kg. With weight loss, subsequent doses were reduced or temporarily withheld until weight was sufficiently recovered. All rats were monitored for body weight, activity, and amount of ascites; hepatic encephalopathy score; and blood measurement of bilirubin, albumin, ammonia, and international normalized ratio.

Cirrhotic rats without liver failure received 13–14 weeks of treatment and a total dose of 1.3 \pm 0.1 mL of CCl₄. Laboratory tests and ascites resolved quickly after discontinuation of treatment. Rats required 2.8 \pm 0.2 mL CCl₄ over 26–28 weeks to generate cirrhosis with irreversible liver failure, and these animals died within 6 weeks after termination of treatment. Livers for this study were collected 4 weeks after the final treatment to eliminate the acute effects of CCl₄ exposure. In some cases, a lobe of the collected liver was excised for hepatocyte isolation.⁶⁵

Mouse hepatocytes for primary cell culture were isolated from C57Bl/6 livers.⁶⁶ RNA was isolated from cells that were freshly isolated or cultured in Dulbecco modified Eagle medium for specified time intervals.

Additional analyses were carried out on frozen F344 rat specimens: pooled 15-day fetal liver and hepatocytes; male livers after BDL for 2, 4, or 12 weeks; and male livers after TAA treatment for 5 months (+5 weeks without treatment) or 6 months (+1 week without treatment).^{67,68}

Cell Isolation and Culture

Stellate cells were isolated from mice as previously described.⁶⁹ Briefly, livers received in situ perfusion with pronase (Roche) followed by collagenase (Roche); dispersed cell suspensions were then layered on a discontinuous density gradient of 8.2 and 15.6% Histodenz. RNA was isolated from freshly prepared cells.

RNA Analysis and Cloning

RNA purification and random primer directed cDNA synthesis for RNA-seq and RT-PCR were previously described.²⁶ Cloning of *Hnf4a-us1-3* was carried out using an Ambion FirstChoice RLM- RACE kit according to the manufacturer's specifications. Primers are listed in Table 3.

RNA-seq Data Analysis

RNA isolation from liver and library construction after random primer cDNA synthesis were previously described.²⁶ Libraries received paired-end sequencing, and FASTQ reads were aligned with RNASTAR⁷⁰ to the rat rn5 or mouse mm9 genome. RNASTAR or GenPlay software⁷¹ was used for reads/transcript quantification using RefSeq rn5 and mm9 annotations. The latter program summed the fractions of reads that overlapped with exons and provided more sensitive quantification of low abundance transcripts. Extraneous transcripts (eg, ribosomal RNA, mitochondrial RNA, and small RNA) were filtered out, and genes with multiple transcripts were simplified to the most abundant isoform. Division by transcript length (kb) converted read counts to molecule counts (reads/kb). Libraries received linear normalization to match the sum of all transcripts in this compilation (the total transcriptome). Where applicable, values for individual or groups of transcripts are displayed as a transcript fraction of this transcriptome. Elsewhere, the values were converted to transcripts/cell by normalizing to Alb mRNA (\sim 20,000 transcripts/cell). For each experimental condition, average transcript values were calculated from 2–3 independent libraries.

Transcriptional analysis of mouse hepatocytes used RNA-seq libraries described in Goldstein et al.³⁹ In this study, hepatocytes were cultured in Dulbecco modified Eagle medium for 24 hours after isolation. If treated, they received 10 ng/mL of IL1, IL6, or a combination for the final 2 hours. Our additional studies used hepatocytes that were freshly isolated or cultured in Dulbecco modified Eagle medium for specified time intervals.

FASTQ libraries were downloaded from the SRA-NCBI database: Control, SRR5353200, SRR5353201; IL1, SRR5353202, SRR5353203; IL6, SRR5353206, SRR5353207; IL1 + IL6, SRR5353208, SRR5353209.

Cell-specific Expression Within the Liver Transcriptome

To assess the gene expression of individual cell types, deep RNA-seq libraries were prepared from freshly isolated stellate cells or obtained from published studies of mouse liver (whole liver,²⁶ cholangiocytes,²⁹ sinusoidal endothelium,⁷² and Kupffer cells⁷³) and other tissues (fibroblasts,⁷⁴

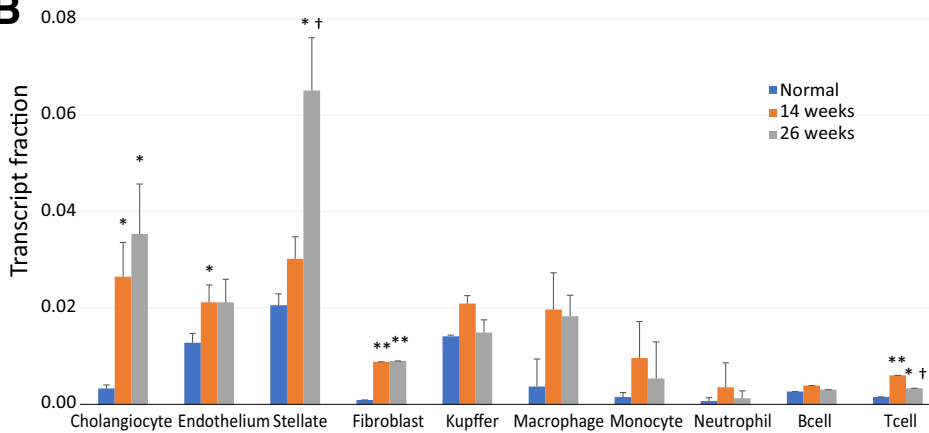
macrophages,⁷⁵ monocytes,⁷⁶ neutrophils,⁷⁵ B cells,⁷⁷ and T cells⁷⁸). Mouse liver data were used for this analysis because comparable studies of rat were not available.

Multiple published studies were compared to find sets with the best alignment to normal liver. FASTQ data sets were aligned, quantified, filtered, and normalized as above

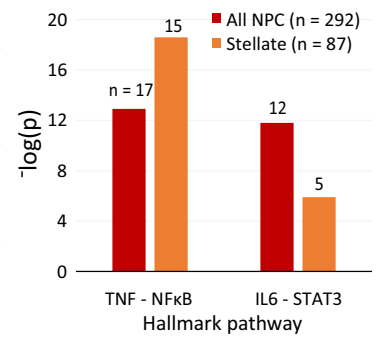
A

Cholangiocyte	Endothelium	Stellate	Fibroblast	Kupffer	Macrophage	Monocyte	Neutrophil	B cell	T cell
Grhl2	Cdh5	Icam1	Col5a2	C1qc	C3ar1	Cx3cr1	Mmp9	Prkcb	Lck
Misp	Pde2a	Mafk	Aebp1	Aif1	Arl11	Gpr141	Alox5	Cd22	Gimap7
Krt19	Flt4	Kcnj8	Angpt4	Lst1	Lat2		Gapd	Aff3	Nkg7
Sema5a	Pecam1	Adora2a	Cacna1g	Ly86	Dpep2		Epx	Cxcr5	Ubash3a
St14	Tek	Tnip1	Dkk2	Ckif	Chst11		Padi4		Cd8a
Il17re	Adgrl4								Cd2
	Jam2								Bcl11b
	Rasip1								
	Flt1								
	Arhgef15								
	Afap111								
	Kank3								
	Shank3								

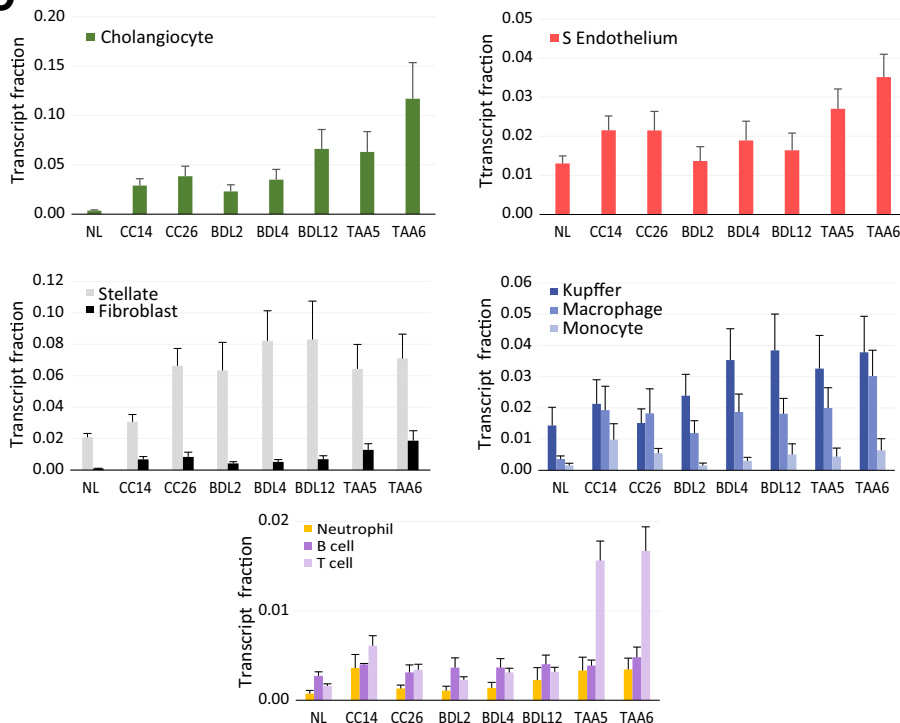
B



D



C



E

NPC type	Gene	TNF-NFkB	IL6-STAT
Endothelium	<i>Edn1</i>	+	
	<i>Socs1</i>		+
	<i>Cntfr</i>		+
	<i>Cd36</i>		+
Stellate	<i>Dusp4</i>	+	
	<i>Cxcl2</i>	+	
	<i>Gem</i>	+	
	<i>Olr1</i>	+	
	<i>Fjx1</i>	+	
	<i>Msc</i>	+	
	<i>Cxcl1</i>	+	+
	<i>Tnfrsf21</i>		+
	<i>Nr4a3</i>	+	
	<i>Cebpd</i>	+	
<i>Ccl2</i>	+		
Kupffer	<i>Ccl7</i>		+
	<i>Gfpt2</i>	+	
	<i>Tnfaip6</i>	+	
	<i>Tnfrsf12a</i>		+
	<i>Cxcl3</i>	+	+
	<i>Spsb1</i>	+	
	<i>Phlda1</i>	+	
Neutrophil	<i>Pmepa1</i>	+	
	<i>Ebi3</i>		+
	<i>Pf4</i>		+
Neutrophil	<i>Cxcl13</i>		+
	<i>Il1r2</i>		+

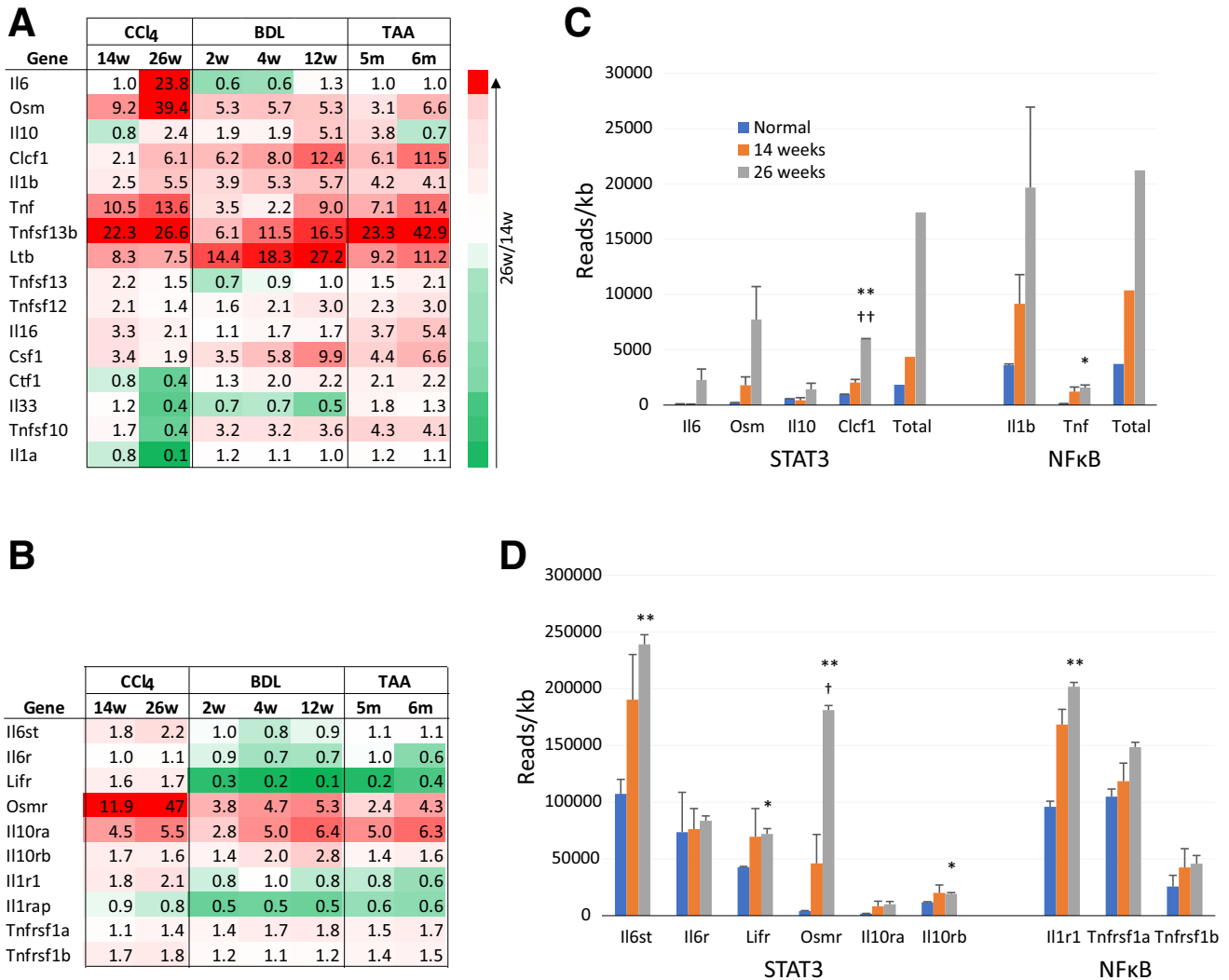


Figure 11. Cytokines and receptors that activate STAT3 or NF κ B. (A) Cytokine expression. Transcripts with 2-fold change in any fibrosis/cirrhosis group. Whole liver RNA-seq values are displayed as ratios of treatment to normal, ranked by the ratio of 26-week to 14-week expression. (B) Quantification of cytokines that increase in CCl₄-induced cirrhosis. (C and D) Receptor expression. *Osmr* was selectively induced in CC26. Most others were well-expressed in normal liver. *P* vs control, * < .05, ***P* < .01; vs 14 weeks, † < .05, †† < .01.

(Supplementary Table 7). For each transcript, the comparison of normalized whole liver with cell-specific libraries was used to identify transcripts that were specific for individual non-hepatocytic cell types. To apply this mouse data resource to rat, a subset of transcripts with common annotation in both species was selected. The transcripts

Figure 10. (See previous page). Quantification of cell types during cirrhosis progression. (A) Non-reactive gene signatures for cell counting. RNA-seq transcriptome analysis identified mouse genes that predominantly represented single-cell types (Supplementary Table 7). Cell counting signatures for rat consisted of genes from the cell-type sets that showed near-median changes, indicating stable gene expression, in experimental groups treated with CCl₄, BDL, or TAA. These signatures were used to quantify cell populations (as fractions of the total transcriptome) and to normalize NPC gene expression (Supplementary Table 8). (B) Progressive changes in NPC transcriptome fractions after CCl₄ treatment. For each cell-type signature, the gene ratios of whole-liver to cell-specific expression were averaged to determine the transcript fraction of the cell-type population. The plot shows mean, standard deviation, and *t* test *P* values: *P* vs control, * < .05, ** < .01; vs 14-week cirrhosis, †*P* < .05. (C) Comparison of NPC cell populations in 3 fibrosis/injury models. CCl₄ data are the same as B. The plots show mean and standard deviation. (D) Cell-normalized NPC responses to IL1-NF κ B and IL6-STAT3 signaling. Cell-specific gene expressions were normalized to cell number and clustered (Supplementary Table 8), generating a set of 292 NPC-specific genes selectively up-regulated in CC26 (normalized stimulation >1.7 fold). NF κ B and STAT3 signaling profiles showed the most significant correlations (<http://www.gsea-msigdb.org>), displayed for the full set of NPC genes and the 87-gene stellate cell subset. *n*, the number of matching genes. (E) IL1-NF κ B and IL6-STAT3 responsive NPC genes identified by gene set enrichment analysis. Cytokines and growth factors, *red*; receptors, *green*; TFs, *blue*.

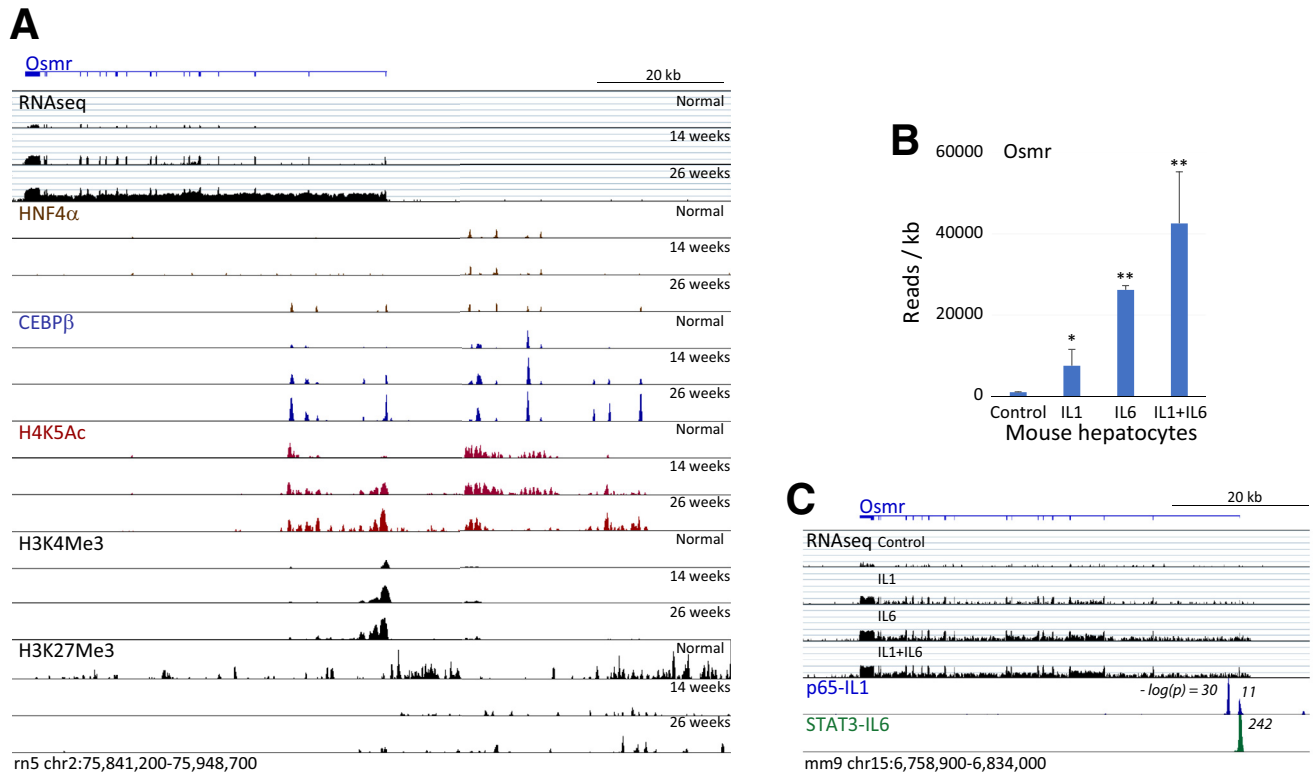


Figure 12. RNA-seq and ChIP-seq characterization of *Osmr*. (A) Rat *Osmr* regulation. In CC26, the gene showed (1) increased transcripts; (2) loss of repressive H3K27Me3 over upstream, promoter, and proximal regions; (3) increase of promoter-activating H3K4Me3 and (4) enhancer-activating H4K5Ac; and (5) de novo or increased binding of HNF4 α and CEBP α within enhancers. (B) IL1 and IL6 induced strong additive stimulation of *Osmr* expression in cultured mouse hepatocytes. (C) ChIP-seq and RNA-seq analysis of *Osmr* activation in cultured mouse hepatocytes. Note one STAT3 and two p65 binding peaks near the mouse promoter (binding significance indicated by $-\log(p)$ values). In A and C, RNA-seq and ChIP-seq data are displayed on log and linear scales, respectively. Histograms show mean and standard deviation: P vs control, * < .05, ** < .01.

were further screened to eliminate those that were depleted from isolated rat liver hepatocytes. The cell-specific genes were then compared in normal liver and 7 cirrhosis conditions to find a median-level gene signature for each cell type, ie, genes neither up- or down-regulated and thus proportional to the number of expressing cells (Figure 8A, Supplementary Table 8). The transcriptome fractions of cell and total liver were calculated for each signature gene. The ratio of those values represented the proportion of the cell-type transcriptome within the whole liver transcriptome. For each cell-type signature, the values for individual genes were averaged to approximate the content of the cell-specific transcriptome within the whole liver transcriptome (Figure 8B and C).

FASTQ libraries were downloaded from the SRA-NCBI database: whole liver (SRR6335223, SRR6335224) and isolated hepatocyte (SRS2725640, SRS3489136)²⁶; cholangiocyte (SRR6392083, SRR6392084, SRR6392085)²⁹; sinusoidal endothelium (SRR5920415, SRR5920416, SRR5920417)⁷²; fibroblast (SRR847341)⁷⁴; Kupffer cell (SRR7519573, SRR7519574, SRR7519575)⁷³; peritoneal macrophage (SRR1177046, SRR1177047)⁷⁵; monocyte (SRR7163783, SRR7163784, SRR7163785)⁷⁶; neutrophil (SRR1177062, SRR1177063)⁷⁵; quiescent follicular B cells

(SRR3724513, SRR3724514)⁷⁷; and unstimulated cytotoxic T lymphocytes (SRR5520192).⁷⁸

ChIP-seq Analysis

Chromatin preparation, immunoprecipitation, and library preparation were previously described.²⁶ ChIP-seq libraries were aligned to the rn5 or mm9 genomes with BWA. Rat libraries were also constructed from control immunoprecipitations with normal serum to define nonspecific peaks. A filter to remove nonspecific peak regions from rn5 alignments was prepared from these control libraries as previously described (available on request).²⁶ These regions were subtracted from all subsequent analysis using BEDtools.⁷⁹ All ChIP-seq analyses combined multiple libraries for each experimental condition. Antibodies were HNF4a sc-8987, CEBPb sc-150 (Santa Cruz Biotechnology, Dallas, TX); and H4K5Ac #39170, H3K4me3 #39915, and H3K27me3 #61017 (Active Motif, Carlsbad, CA).

Compilation and Analysis of ChIP-seq Peak Sets

After filtering, HNF4 α , CEBP β , H4K5Ac, H3K4Me3, and H3K27Me3 peak sets were compiled for normal liver, CC14, and CC26 by using MACS2 and 2–3 replicates for each

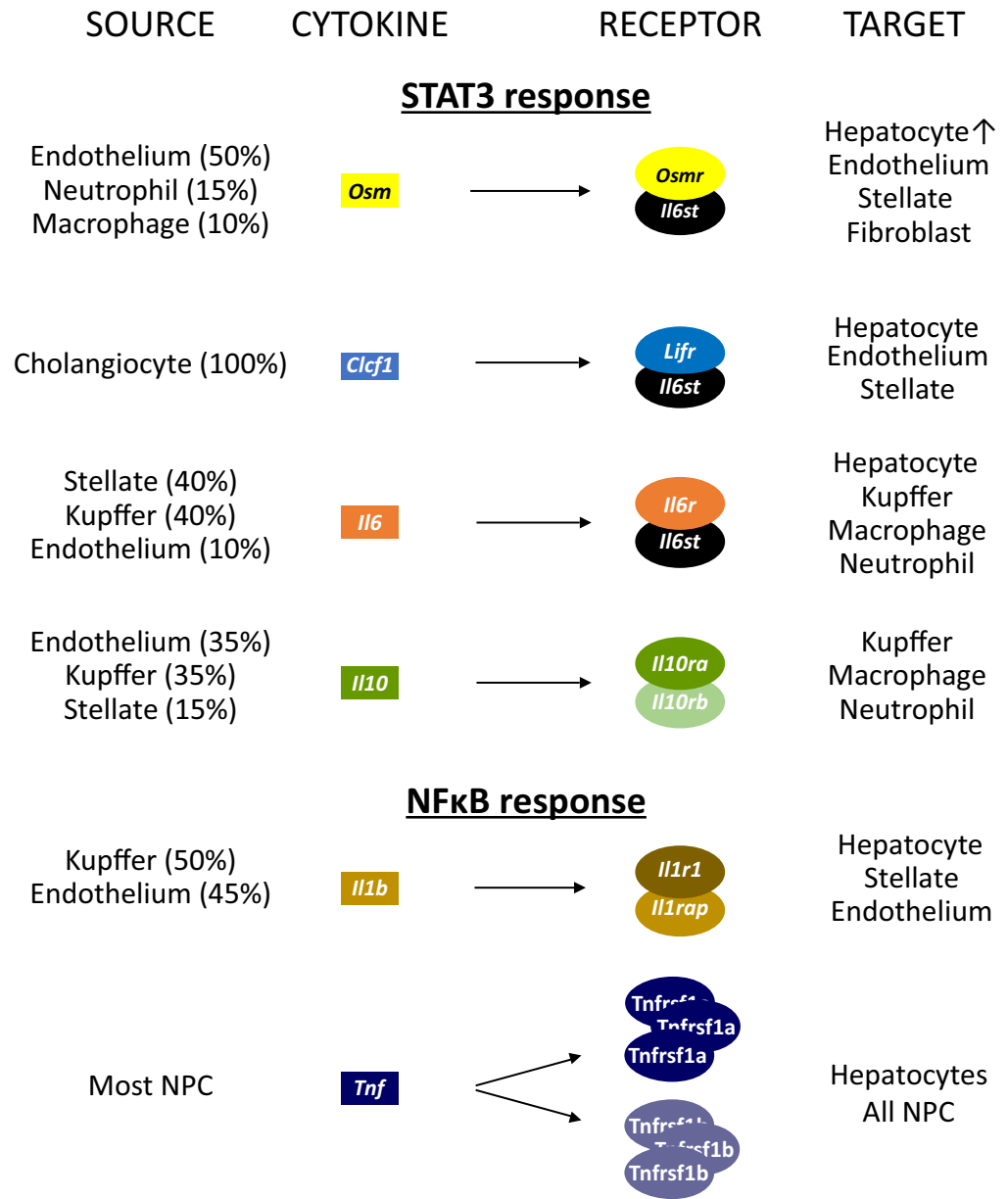


Figure 13. Reactive intra-hepatic signaling of STAT3 and NF κ B responses. Cytokine genes are ranked by their expression level in CC26. Main expressing cells are listed with their contributions to total expression in normal liver. In progression to CC14 and CC26, expression of all receptors stayed the same or increased. *Osmr* was not expressed in normal hepatocytes but strongly induced (arrow) by prior stimulation with other cytokines.

experimental condition.⁸⁰ For quantification, all HNF4 α peak sets were combined with MACS2 into a common peak set. This common set was then used to score HNF4 α peak area with GenPlay in separate compilations from each experimental condition. The peaks were also scored with GenPlay for local H4K5Ac binding in a 1000-bp window around the HNF4 α peak summit. For both HNF4 α and H4K5Ac quantifications, the data sets for each experimental condition were normalized to each other using the median values. Filtering out weak binding of HNF4 α and H4K5Ac (the bottom 10% of the maximum detected levels) reduced the set to 19,646 transcriptional active peaks. CEBP β , H3K4Me3, and H3K27Me3 ChIP-seq data were used for qualitative assessments. The data displays were normalized to the median values of peak sets (Figures 1, 4, 7, and 8). Mouse ChIP-seq sets from Goldstein et al³⁹ were used to

compile STAT3 and NF κ B-p65 peaks. These compilations received analysis as above, except that local H3K27Ac was used to mark transcriptionally active peaks. Binding site motifs were analyzed with MEME Suite programs MEME-ChIP, FIMO, and AME (<https://meme-suite.org/meme/>). HNF4 α peaks were associated with the transcription start of the nearest expressed gene using RnaChipIntegrator (<https://github.com/fls-bioinformatics-core/RnaChipIntegrator>). For correlation of gene expression with changes in HNF4 α binding, the areas of all peaks associated with a single gene were summed. Ratios of these sums were calculated for each experimental condition.

FASTQ files were downloaded from the SRA-NCBI database: STAT3 NT, SRR5353181, SRR5353180; STAT3 IL1, SRR5353183, SRR5353182; STAT3 IL6, SRR5353185, SRR5353184; STAT3 IL1 + IL6, SRR5353187, SRR5353186;

Table 3. RT-PCR and Cloning Primers

Species	Gene	Forward primer	Reverse primer
Rat	<i>Hnf4a</i> (P1)	TGGACCCAGCCTACACCACCC	GGTTGGCACCTTCAGATGGGG
Rat	<i>Hnf4a</i> (P2)	CGGGGCTCCAGTGGCGAGT	CCACAGATGGCACACAGGGCA
Rat	<i>Hnf4a-us</i> RACE	CAAGCAGCCACCTGGCCTCA	
Rat	<i>Hnf4a-us3</i>	CCCATTCTTATCTGAGAGGACCACC	GGATTGGGAAGAGACAGAGGAGGA
Rat	<i>Hnf4a-us3</i> unspliced	CCCATTCTTATCTGAGAGGACCACC	CCAGGAGGTCCAGATGGGACTTAGC
Mouse	<i>Hnf4a</i> (P1)	TGGACCCAGCCTACACCACCC	GGTTGGCACCTTCAGATGGGGAC
Mouse	<i>Hnf4a</i> (P2)	CGGGGCTCCAGTGGCGAGT	CCACAGATGGCACACAGGGCA
Mouse	<i>Hnf4aos</i>	CCCGTTCTTATCTGAGAGGACCCT	CTTCTGGCCTCCAATGGACACAC
Mouse	<i>Hnf4aos</i> unspliced	CCCGTTCTTATCTGAGAGGACCCT	CCAGGAGGTCTTGATGGGACTTAGC

p65 IL1, SRR5353188; H3K27ac NT, SRR5353160, SRR5353161, SRR5353162; H3K27ac IL1 SRR5353163, SRR5353164, SRR5353165; H3K27ac IL6 SRR5353166, SRR5353167, SRR5353168; H3K27Ac IL1 + IL6 SRR5353169, SRR5353170, SRR5353171.

Data Availability

Transcript characterization. Sequences of lncRNA isoforms *Hnf4a-us1* – 3 were submitted to GenBank (MT790745.1, MT790746.1, MT790747.1).

Primary sequencing data were submitted to the SRI-NCI database in projects PRJNA895426 (Mouse Liver Stellate Transcriptome) and PRJNA949711 (Cirrhosis and Liver Failure).

RNA-seq. Lewis rat: Normal (SRR24009503, SRR24009505), CCl₄ 14 weeks (SRR24009499, SRR24009500, SRR24009502); CCl₄ 26 weeks (SRR24009497, SRR24009498), normal hepatocytes (SRR24009504), CCl₄ 14-week hepatocytes (SRR24009502). F344 rat: Normal (SRR24065129, SRR24065130), BDL 2 weeks, (SRR24065124, SRR24065125), BDL 4 weeks (SRR24065122, SRR24065123), BDL 12 weeks (SRR24065120, SRR24065121), TAA 5 months + 5 weeks recovery (SRR24065118, SRR24065119), TAA 6 months + 1 week recovery (SRR24065127, SRR24065128), fetal liver 15 days (SRR24065126). C57Bl/6 mouse hepatocytes: 0 hour (SRR24060902, SRR24060903); 3 hour (SRR24060900, SRR24060901); 6 hour (SRR24060898, SRR24060899); 12 hour (SRR24060897); 24 hour (SRR24060896). Stellate cells: (SRR22084560, SRR22084559, SRR22084558, SRR22084557).

ChIP-seq. CEBP β : normal (SRR24037239, SRR24037210), 14 weeks (SRR24037237, SRR24037233, SRR24037228), 26 weeks (SRR24037222, SRR24037217). HNF4 α : normal (SRR24037238, SRR24037209), 14 weeks (SRR24037236, SRR24037232, SRR24037226), 26 weeks (SRR24037221, SRR24037215). H3K4Me3: normal (SRR24037227, SRR24037208), 14 weeks (SRR24037235, SRR24037231, SRR24037225), 26 weeks (SRR24037220, SRR24037214). H4K5Ac: normal (SRR24037216, SRR24037207), 14 weeks (SRR24037230, SRR24037224), 26 weeks (SRR24037219, SRR24037213). H3K27Me3:

normal (SRR24037211, SRR24037206); 14 weeks (SRR24037234, SRR24037229, SRR24037223); 26 weeks (SRR24037218, SRR24037212).

Supplementary Material

Note: To access the supplementary material accompanying this article, go to the full text version at <http://doi.org/10.1016/j.jcmgh.2023.11.009>.

References

- Asrani SK, Devarbhavi H, Eaton J, et al. Burden of liver diseases in the world. *J Hepatol* 2019;70:151–171.
- Mansour D, McPherson S. Management of decompensated cirrhosis. *Clin Med (Lond)* 2018;18:s60–s65.
- Schuppan D, Afdhal NH. Liver cirrhosis. *Lancet* 2008; 371:838–851.
- Friedman SL. Liver fibrosis: from bench to bedside. *J Hepatol* 2003;38(Suppl 1):S38–S53.
- Iwakiri Y, Shah V, Rockey DC. Vascular pathobiology in chronic liver disease and cirrhosis: current status and future directions. *J Hepatol* 2014;61:912–924.
- Fausto N. Liver regeneration and repair: hepatocytes, progenitor cells, and stem cells. *Hepatology* 2004; 39:1477–1487.
- Lemasters JL, Jaeschke H. Oxidative stress and inflammation in the liver. In: Arias IM, Alter HJ, Boyer JL, Cohen DE, et al., eds. *The liver: biology and pathobiology*. 6th ed. New York: John Wiley & Sons Ltd, 2020:714–727.
- Kumar R, Mehta G, Jalan R. Acute-on-chronic liver failure. *Clin Med (Lond)* 2020;20:501–504.
- Fontana RJ. Acute liver failure including acetaminophen overdose. *Med Clin North Am* 2008;92:761–794, viii.
- Choudhury A, Jindal A, Maiwall R, et al. Liver failure determines the outcome in patients of acute-on-chronic liver failure (ACLF): comparison of APASL ACLF research consortium (AARC) and CLIF-SOFA models. *Hepatology Int* 2017;11:461–471.
- Jayaraman T, Lee YY, Chan WK, et al. Epidemiological differences of common liver conditions between Asia and the West. *JGH Open* 2020;4:332–339.
- Axley P, Ahmed Z, Arora S, et al. NASH is the most rapidly growing etiology for acute-on-chronic liver failure-related hospitalization and disease burden in the

- United States: a population-based study. *Liver Transpl* 2019;25:695–705.
13. Sundaram V, Jalan R, Shah P, et al. Acute on chronic liver failure from nonalcoholic fatty liver disease: a growing and aging cohort with rising mortality. *Hepatology* 2021;73:1932–1944.
 14. Bassegoda O, Rivera-Esteban J, Serra I, et al. High frequency of acute decompensation and cancer in patients with compensated cirrhosis due to nonalcoholic fatty liver disease: a retrospective cohort study. *Hepatology* 2022;6:3212–3222.
 15. Graupera I, Isus L, Coll M, et al. Molecular characterization of chronic liver disease dynamics: from liver fibrosis to acute-on-chronic liver failure. *JHEP Rep* 2022; 4:100482.
 16. Muriel P, Moreno MG, Hernandez Mdel C, et al. Resolution of liver fibrosis in chronic CCl4 administration in the rat after discontinuation of treatment: effect of silymarin, silibinin, colchicine and trimethylcolchicinic acid. *Basic Clin Pharmacol Toxicol* 2005;96:375–380.
 17. Kobayashi N, Ito M, Nakamura J, et al. Hepatocyte transplantation in rats with decompensated cirrhosis. *Hepatology* 2000;31:851–857.
 18. Liu L, Yannam GR, Nishikawa T, et al. The microenvironment in hepatocyte regeneration and function in rats with advanced cirrhosis. *Hepatology* 2012;55:1529–1539.
 19. Nishikawa T, Bell A, Brooks JM, et al. Resetting the transcription factor network reverses terminal chronic hepatic failure. *J Clin Invest* 2015;125:1533–1544.
 20. Fang B, Mane-Padros D, Bolotin E, et al. Identification of a binding motif specific to HNF4 by comparative analysis of multiple nuclear receptors. *Nucleic Acids Res* 2012; 40:5343–5356.
 21. Yue HY, Yin C, Hou JL, et al. Hepatocyte nuclear factor 4 α attenuates hepatic fibrosis in rats. *Gut* 2010; 59:236–246.
 22. Yang T, Poenisch M, Khanal R, et al. Therapeutic HNF4A mRNA attenuates liver fibrosis in a preclinical model. *J Hepatol* 2021;75:1420–1433.
 23. Argemi J, Latasa MU, Atkinson SR, et al. Defective HNF4 α -dependent gene expression as a driver of hepatocellular failure in alcoholic hepatitis. *Nat Commun* 2019;10:3126.
 24. Guzman-Lepe J, Cervantes-Alvarez E, Collin de l'Hortet A, et al. Liver-enriched transcription factor expression relates to chronic hepatic failure in humans. *Hepatology* 2018;2:582–594.
 25. Gunewardena S, Huck I, Walesky C, et al. Progressive loss of hepatocyte nuclear factor 4 α activity in chronic liver diseases in humans. *Hepatology* 2022; 76:372–386.
 26. Tian J, Marino R, Johnson C, et al. Binding of drug-activated CAR/Nr1i3 alters metabolic regulation in the liver. *iScience* 2018;9:209–228.
 27. Briancon N, Bailly A, Clotman F, et al. Expression of the α 7 isoform of hepatocyte nuclear factor (HNF) 4 is activated by HNF6/OC-2 and HNF1 and repressed by HNF4 α 1 in the liver. *J Biol Chem* 2004; 279:33398–33408.
 28. Torres-Padilla ME, Fougere-Deschatrette C, Weiss MC. Expression of HNF4 α isoforms in mouse liver development is regulated by sequential promoter usage and constitutive 3' end splicing. *Mech Dev* 2001;109:183–193.
 29. Schaub JR, Huppert KA, Kurial SNT, et al. De novo formation of the biliary system by TGF β -mediated hepatocyte transdifferentiation. *Nature* 2018;557:247–251.
 30. Limaye PB, Bowen WC, Orr A, et al. Expression of hepatocyte- and biliary-specific transcription factors in regenerating bile ducts during hepatocyte-to-biliary epithelial cell transdifferentiation. *Comp Hepatol* 2010;9:9.
 31. Tanaka T, Jiang S, Hotta H, et al. Dysregulated expression of P1 and P2 promoter-driven hepatocyte nuclear factor-4 α in the pathogenesis of human cancer. *J Pathol* 2006;208:662–672.
 32. Jiang G, Sladek FM. The DNA binding domain of hepatocyte nuclear factor 4 mediates cooperative, specific binding to DNA and heterodimerization with the retinoid X receptor α . *J Biol Chem* 1997;272:1218–1225.
 33. Kulakovskiy IV, Vorontsov IE, Yevshin IS, et al. HOCO-MOCO: towards a complete collection of transcription factor binding models for human and mouse via large-scale ChIP-Seq analysis. *Nucleic Acids Res* 2018; 46:D252–D259.
 34. Tian J, Mahmood R, Hnasko R, et al. Loss of Nkx2.8 deregulates progenitor cells in the large airways and leads to dysplasia. *Cancer Res* 2006;66:10399–10407.
 35. Li W, Notani D, Ma Q, et al. Functional roles of enhancer RNAs for oestrogen-dependent transcriptional activation. *Nature* 2013;498:516–520.
 36. Thomsen KL, Hebbard L, Glavind E, et al. Non-alcoholic steatohepatitis weakens the acute phase response to endotoxin in rats. *Liver Int* 2014;34:1584–1592.
 37. Denson LA, McClure MH, Bogue CW, et al. HNF3 β and GATA-4 transactivate the liver-enriched homeobox gene. *Hex. Gene* 2000;246:311–320.
 38. Bagu ET, Santos MM. Friend of GATA suppresses the GATA-induced transcription of hepcidin in hepatocytes through a GATA-regulatory element in the HAMP promoter. *J Mol Endocrinol* 2011;47:299–313.
 39. Goldstein I, Paakinaho V, Baek S, et al. Synergistic gene expression during the acute phase response is characterized by transcription factor assisted loading. *Nat Commun* 2017;8:1849.
 40. Mendoza L, Olaso E, Anasagasti MJ, et al. Mannose receptor-mediated endothelial cell activation contributes to B16 melanoma cell adhesion and metastasis in liver. *J Cell Physiol* 1998;174:322–330.
 41. Costa R, Grayson D, Darnell J. Multiple hepatocyte-enriched nuclear factors function in the regulation of transthyretin and α 1-antitrypsin genes. *Mol Cell Biol* 1989;9:1415–1425.
 42. Sladek FM, Zhong WM, Lai E, et al. Liver-enriched transcription factor HNF-4 is a novel member of the steroid hormone receptor superfamily. *Genes Dev* 1990; 4:2353–2365.
 43. Ruse MD Jr, Privalsky ML, Sladek FM. Competitive cofactor recruitment by orphan receptor hepatocyte nuclear factor 4 α 1: modulation by the F domain. *Mol Cell Biol* 2002;22:1626–1638.

44. Radi SH, Vemuri K, Martinez-Lomeli J, et al. HNF4alpha isoforms: the fraternal twin master regulators of liver function. *Front Endocrinol (Lausanne)* 2023;14:1226173.
45. Briancon N, Weiss MC. In vivo role of the HNF4alpha AF-1 activation domain revealed by exon swapping. *EMBO J* 2006;25:1253–1262.
46. Chellappa K, Deol P, Evans JR, et al. Opposing roles of nuclear receptor HNF4alpha isoforms in colitis and colitis-associated colon cancer. *Elife* 2016;5.
47. Sartorelli V, Lauberth SM. Enhancer RNAs are an important regulatory layer of the epigenome. *Nat Struct Mol Biol* 2020;27:521–528.
48. Deniz E, Erman B. Long noncoding RNA (lincRNA), a new paradigm in gene expression control. *Funct Integr Genomics* 2017;17:135–143.
49. Mattick JS. RNA out of the mist. *Trends Genet* 2023;39:187–207.
50. Rinn JL. lncRNAs: linking RNA to chromatin. *Cold Spring Harb Perspect Biol* 2014;6.
51. Bellido Molias F, Sim A, Leong KW, et al. Antisense RNAs influence promoter usage of their counterpart sense genes in cancer. *Cancer Res* 2021;81:5849–5861.
52. Schaffner G, Schirm S, Muller-Baden B, et al. Redundancy of information in enhancers as a principle of mammalian transcription control. *J Mol Biol* 1988;201:81–90.
53. Kim TK, Maniatis T. The mechanism of transcriptional synergy of an in vitro assembled interferon-beta enhancosome. *Mol Cell* 1997;1:119–129.
54. Vuong LM, Chellappa K, Dhahbi JM, et al. Differential effects of hepatocyte nuclear factor 4alpha isoforms on tumor growth and T-cell factor 4/AP-1 interactions in human colorectal cancer cells. *Mol Cell Biol* 2015;35:3471–3490.
55. Biddie SC, John S, Sabo PJ, et al. Transcription factor AP1 potentiates chromatin accessibility and glucocorticoid receptor binding. *Mol Cell* 2011;43:145–155.
56. Waters CT, Gisselbrecht SS, Sytnikova YA, et al. Quantitative-enhancer-FACS-seq (QeFS) reveals epistatic interactions among motifs within transcriptional enhancers in developing *Drosophila* tissue. *Genome Biol* 2021;22:348.
57. Parviz F, Matullo C, Garrison WD, et al. Hepatocyte nuclear factor 4alpha controls the development of a hepatic epithelium and liver morphogenesis. *Nat Genet* 2003;34:292–296.
58. Woolbright BL, Jaeschke H. Novel insight into mechanisms of cholestatic liver injury. *World J Gastroenterol* 2012;18:4985–4993.
59. Wang H, Zhang H, Wang Y, et al. Embelin can protect mice from thioacetamide-induced acute liver injury. *Biomed Pharmacother* 2019;118:109360.
60. Arroyo V, Angeli P, Moreau R, et al. The systemic inflammation hypothesis: towards a new paradigm of acute decompensation and multiorgan failure in cirrhosis. *J Hepatol* 2021;74:670–685.
61. Albillos A, de Gottardi A, Rescigno M. The gut-liver axis in liver disease: pathophysiological basis for therapy. *J Hepatol* 2020;72:558–577.
62. Boelen A, Kwakkel J, Alkemade A, et al. Induction of type 3 deiodinase activity in inflammatory cells of mice with chronic local inflammation. *Endocrinology* 2005;146:5128–5134.
63. Dierssen U, Beraza N, Lutz HH, et al. Molecular dissection of gp130-dependent pathways in hepatocytes during liver regeneration. *J Biol Chem* 2008;283:9886–9895.
64. Alonzi T, Fattori E, Cappelletti M, et al. Impaired Stat3 activation following localized inflammatory stimulus in IL-6-deficient mice. *Cytokine* 1998;10:13–18.
65. Seglen PO. Preparation of isolated rat liver cells. *Methods Cell Biol* 1976;13:29–83.
66. Kost DP, Michalopoulos GK. Effect of 2% dimethyl sulfoxide on the mitogenic properties of epidermal growth factor and hepatocyte growth factor in primary hepatocyte culture. *J Cell Physiol* 1991;147:274–280.
67. Yovchev MI, Locker J, Oertel M. Biliary fibrosis drives liver repopulation and phenotype transition of transplanted hepatocytes. *J Hepatol* 2016;64:1348–1357.
68. Yovchev MI, Xue Y, Shafritz DA, et al. Repopulation of the fibrotic/cirrhotic rat liver by transplanted hepatic stem/progenitor cells and mature hepatocytes. *Hepatology* 2014;59:284–295.
69. Du K, Oh SH, Dutta RK, et al. Inhibiting xCT/SLC7A11 induces ferroptosis of myofibroblastic hepatic stellate cells but exacerbates chronic liver injury. *Liver Int* 2021;41:2214–2227.
70. Widmann J, Stombaugh J, McDonald D, et al. RNAS-TAR: an RNA STructural Alignment Repository that provides insight into the evolution of natural and artificial RNAs. *RNA* 2012;18:1319–1327.
71. Lajugie J, Bouhassira EE. GenPlay, a multipurpose genome analyzer and browser. *Bioinformatics* 2011;27:1889–1893.
72. Duan JL, Ruan B, Yan XC, et al. Endothelial Notch activation reshapes the angiocrine of sinusoidal endothelia to aggravate liver fibrosis and blunt regeneration in mice. *Hepatology* 2018;68:677–690.
73. Scott CL, T'Jonck W, Martens L, et al. The transcription factor ZEB2 is required to maintain the tissue-specific identities of macrophages. *Immunity* 2018;49:312–325 e5.
74. Kumar R, DiMenna L, Schrode N, et al. AID stabilizes stem-cell phenotype by removing epigenetic memory of pluripotency genes. *Nature* 2013;500:89–92.
75. Hutchins AP, Takahashi Y, Miranda-Saavedra D. Genomic analysis of LPS-stimulated myeloid cells identifies a common pro-inflammatory response but divergent IL-10 anti-inflammatory responses. *Sci Rep* 2015;5:9100.
76. Shaw TN, Houston SA, Wemyss K, et al. Tissue-resident macrophages in the intestine are long lived and defined by Tim-4 and CD4 expression. *J Exp Med* 2018;215:1507–1518.
77. Saelee P, Kearly A, Nutt SL, et al. Genome-wide identification of target genes for the key B cell transcription factor Ets1. *Front Immunol* 2017;8:383.
78. Klein-Hessling S, Muhammad K, Klein M, et al. NFATc1 controls the cytotoxicity of CD8(+) T cells. *Nat Commun* 2017;8:511.
79. Quinlan AR, Hall IM. BEDTools: a flexible suite of utilities for comparing genomic features. *Bioinformatics* 2010;26:841–842.
80. Feng J, Liu T, Qin B, et al. Identifying ChIP-seq enrichment using MACS. *Nat Protoc* 2012;7:1728–1740.

Received June 2, 2023. Accepted November 14, 2023.

Correspondence

Address correspondence to: Joseph Locker, MD, PhD, Department of Pathology, School of Medicine, University of Pittsburgh, BST South, Room 421, 200 Lothrop Street, Pittsburgh, Pennsylvania 15213. e-mail: jlocker@upmc.edu.

Acknowledgments

Current address for Marta Melis: Department of Pharmacology, Weill Cornell Medical College of Cornell University, New York, New York.

CRediT Authorship Contributions

Marta Melis (Conceptualization: Supporting; Data curation: Supporting; Formal analysis: Supporting; Investigation: Lead; Writing – original draft: Supporting; Writing – review & editing: Supporting)

Rebecca Marino (Conceptualization: Supporting; Data curation: Supporting; Formal analysis: Supporting; Investigation: Supporting; Software: Supporting)

Jianmin Tian (Investigation: Supporting; Methodology: Supporting)

Carla Johnson (Investigation: Supporting; Project administration: Supporting)

Rahil Sethi (Data curation: Supporting; Formal analysis: Supporting; Software: Supporting; Writing – review & editing: Supporting)

Michael Oertel (Funding acquisition: Supporting; Investigation: Supporting; Methodology: Supporting; Resources: Supporting)

Ira J. Fox (Conceptualization: Supporting; Funding acquisition: Equal; Investigation: Supporting; Methodology: Supporting; Resources: Equal; Writing – review & editing: Supporting)

Joseph Locker (Conceptualization: Lead; Formal analysis: Lead; Funding acquisition: Equal; Investigation: Supporting; Methodology: Equal; Project administration: Lead; Visualization: Lead; Writing – original draft: Lead; Writing – review & editing: Lead)

Conflicts of interest

This author discloses the following: IJF was inventor on a patent application that describes the use of transcription factors to treat chronic liver failure (US20140249209), inventor on a provisional patent application related to methods to enhance hepatic function in human failing livers (PCT/US2020/055500), and has a financial interest in Von Baer Wolff, Inc, a company focused on biofabrication of autologous human hepatocytes from stem cell technology and reprogramming hepatocytes in liver failure. All interests are managed by the Conflict of Interest Office at the University of Pittsburgh in accordance with their policies. The remaining authors disclose no conflicts.

Funding

Supported by National Institutes of Health grants R01 DK099320 (IJF and JL), R01 CA104292 (JL), and R01 DK090325 (MO).